

THE GAMMA SYSTEM OF THE NITRIC-OXIDE ISOTOPOMERS



CENTRE FOR NEWFOUNDLAND STUDIES

**TOTAL OF 10 PAGES ONLY
MAY BE XEROXED**

(Without Author's Permission)

DUANXIANG WANG, B.Sc.



THE GAMMA SYSTEM OF THE NITRIC-OXIDE ISOTOPOMERS

$^{14}\text{N}^{16}\text{O}$, $^{15}\text{N}^{16}\text{O}$, $^{14}\text{N}^{18}\text{O}$ AND $^{15}\text{N}^{18}\text{O}$

By

©Duanxiang Wang

B. Sc., Tongji University, China

A THESIS SUBMITTED TO THE SCHOOL OF GRADUATE
STUDIES IN PARTIAL FULFILLMENT OF THE
REQUIREMENTS FOR THE DEGREE OF
MASTER OF SCIENCE

DEPARTMENT OF PHYSICS
MEMORIAL UNIVERSITY OF NEWFOUNDLAND
JULY 1992

ST. JOHN'S

NEWFOUNDLAND



National Library
of Canada

Acquisitions and
Bibliographic Services Branch

395 Wellington Street
Ottawa, Ontario
K1A 0N4

Bibliothèque nationale
du Canada

Direction des acquisitions et
des services bibliographiques

395, rue Wellington
Ottawa (Ontario)
K1A 0N4

Number: 130-100-1000

Date: 1998-01-01

The author has granted an irrevocable non-exclusive licence allowing the National Library of Canada to reproduce, loan, distribute or sell copies of his/her thesis by any means and in any form or format, making this thesis available to interested persons.

The author retains ownership of the copyright in his/her thesis. Neither the thesis nor substantial extracts from it may be printed or otherwise reproduced without his/her permission.

L'auteur a accordé une licence irrévocable et non exclusive permettant à la Bibliothèque nationale du Canada de reproduire, prêter, distribuer ou vendre des copies de sa thèse de quelque manière et sous quelque forme que ce soit pour mettre des exemplaires de cette thèse à la disposition des personnes intéressées.

L'auteur conserve la propriété du droit d'auteur qui protège sa thèse. Ni la thèse ni des extraits substantiels de celle-ci ne doivent être imprimés ou autrement reproduits sans son autorisation.

ISBN 0-315-78106-8

Canada

DEDICATED TO MY PARENTS

ACKNOWLEDGMENTS

I am greatly indebted to my supervisor Professor S. P. Reddy for suggesting the research project and for his constant encouragement and guidance through all aspects of this thesis.

I wish to express my thanks to Mr. C. Haridass for his initial help in operation of the apparatus and also for useful discussions in the computational work. I would like to thank Dr. C. V. V. Prasad for his constructive suggestions and Dr. K. P. Huber for providing some reference materials.

I extend my thanks to the following technical personnel for their assistance: Messrs. M. Ryan, R. Guest and R. Bradley of the Physics Department for machine shop work, some drafting work and some photographic work, respectively, and Messrs T. Perks and M. Hatswell of the Technical Service for skillful glass blowing. I also wish to thank the staffs of the Computing Services of the University for their assistance.

The financial assistance received from the Physics Department and Dr. Reddy's NSERC grant is gratefully appreciated.

I would like to extend my thanks to my wife, Lina, for her help and understanding. Finally, and most of all, my thanks go to my parents for their constant spiritual support and unflinching encouragement.

ABSTRACT

The spectra of the gamma ($A^2\Sigma^+ - X^2\Pi_r$) system of the nitric-oxide isotopomers $^{14}\text{N}^{16}\text{O}$, $^{15}\text{N}^{16}\text{O}$, $^{14}\text{N}^{18}\text{O}$ and $^{15}\text{N}^{18}\text{O}$, excited in the anode glow of a two-column hollow-cathode discharge tube of special design (Reddy and Prasad, J. Phys. E. Sci. Instr. **22**, 306, 1989), were photographed in the spectral region 2140-2730 Å on a 2 m Bausch and Lomb spectrograph under medium resolution and the spectrum of $^{15}\text{N}^{18}\text{O}$ was also recorded on a 3.1 m Jarrell-Ash spectrograph under high resolution. The spectrum of $^{14}\text{N}^{16}\text{O}$ was obtained from the natural presence of nitrogen-14 and oxygen-16 of low pressure air in the discharge tube. The spectra of $^{15}\text{N}^{16}\text{O}$ and $^{14}\text{N}^{18}\text{O}$ were produced by admitting nitrogen-15 and oxygen-18 into the discharge tube, respectively. The spectrum $^{15}\text{N}^{18}\text{O}$ was produced by admitting a mixture of nitrogen-15 and oxygen-18 into the same discharge tube. The gamma system has been observed for the first time for $^{15}\text{N}^{18}\text{O}$.

For each of the isotopomers, six bands, namely, 1-0, 0-0, 0-1, 0-2, 0-3 and 0-4, each having four heads P_{12ee} , P_{22ff}/Q_{12ef} , P_{11ee} and P_{21ff}/Q_{11ef} , have been observed. The vibrational structures of the observed bands have been analyzed from the wavenumber data of the band heads of all the isotopomers of NO. In each case $\Delta G(1/2)$ of the $A^2\Sigma^+$ state and vibrational constants ω_e and $\omega_e x_e$ of the $X^2\Pi_{1/2}$ and $X^2\Pi_{3/2}$ components of the ground electronic state have been determined.

The rotational structure of the individual 0-1, 0-2 and 0-3 bands of the gamma system of $^{15}\text{N}^{18}\text{O}$, photographed under high resolution, has been analyzed using the effective Hamiltonian proposed by Brown *et al* (J. Mol. Spectrosc. **74**, 294, 1979) and a unique set of molecular constants has been obtained by the method of merging. The derived molecular constants in cm^{-1} of $^{15}\text{N}^{18}\text{O}$ are:

$$A^2\Sigma^+ : \Delta G(1/2) \quad 2237.1$$

$$X^2\Pi : \omega_e \quad 1819.15; \omega_e x_e \quad 12.870; B_e = 1.55644; \alpha_e = 0.015343; D_e = 4.5574 \times 10^{-6}.$$

Also obtained for the $X^2\Pi$ state are the values of A_v , A_{Dv} , p_v , q_v for $v = 1, 2$, and 3 levels.

Table of Contents

ACKNOWLEDGMENTS	iii
ABSTRACT	iv
1 INTRODUCTION	1
1.1 Importance of Molecular Spectra	1
1.2 Significance of Nitric Oxide	2
1.3 Electronic Configurations and Potential Energy Curves of NO	1
1.4 Previous Work on the γ ($A^2\Sigma^+ - X^2\Pi$) System and the Infrared Vibration-Rotation and Pure Rotation Spectra in the $X^2\Pi$ state of Nitric Oxide	7
1.5 Present work	9
2 EXPERIMENTAL TECHNIQUES	10
2.1 Two-Column Hollow-Cathode Discharge Tube	10
2.2 Mechanism of a Hollow-Cathode Discharge	15
2.3 Spectrographs	16
2.4 Experimental Procedure	20
2.5 Measurement of Spectra	21
3 THEORETICAL ASPECTS FOR THE ANALYSIS OF THE NO γ SYSTEM	23
3.1 Vibrational and Rotational Structures of Electronic Band Systems	23
3.2 Method of Rotational Analysis	31

3.3	The Rotational Structure of a Band of a ${}^2\Sigma^- - {}^2\Pi_r$ Transition	35
4	ANALYSIS OF THE SPECTRA OF THE γ SYSTEM OF NITRIC OXIDE	39
4.1	Vibrational Analysis	39
4.2	Rotational Analysis of the 0-1, 0-2 and 0-3 bands of ${}^{15}\text{N } {}^{18}\text{O}$	52
4.3	Summary	78
	Bibliography	79

Chapter 1

INTRODUCTION

1.1 Importance of Molecular Spectra

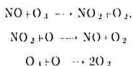
Along with the development of quantum mechanics in late 1920's, great progress was made in the experimental studies of the electronic spectra of diatomic molecules and their theoretical understanding. From the investigation of the electronic spectrum of a molecule, its electronic, vibrational and rotational energy levels can be obtained very precisely. Also, information about the molecular electronic structure, and vibration and rotation of its nuclei can be obtained. Properties such as chemical valence can be understood from the electronic structure. From a knowledge of the vibrational frequencies and the anharmonicities of a molecule, the forces between the constituent atoms as well as its dissociation energy can be calculated. Detailed rotational analysis of the electronic bands of a molecule gives accurate values of the moments of inertia and internuclear separations in various energy states, and provides information on the nature of the coupling between the orbital and spin motions of its electrons and rotational motion of the molecule, as well as information about the possible perturbations between the energy levels of different electronic states. From the known vibrational and rotational partition functions, several thermodynamic quantities can be estimated. From a knowledge of the vibrational and rotational constants of the electronic states of a molecule, quantities such as Franck-Condon factors which are proportional to the intensity of the bands can be estimated.

Molecular spectra also play an important role in the investigation of the atmospheric and astrophysical phenomena such as molecular absorption of the solar radiation in the earth's atmosphere, emission spectra of aurora, emission from the night sky and twilight, all of which are produced in the upper layers of the atmosphere. These molecular spectra provide information about the physical conditions and the composition of the atmospheric layers. The temperature and height of various atmospheric layers can be estimated from the intensity distribution in the bands of the atmospheric spectra. The comet tails give emission spectra of neutral molecules and molecular ions. The temperature of the stars can be estimated from their spectra and the stars can be classified according to their temperatures (see Herzberg, 1950). From the spectra of celestial objects, abundance ratios of isotopomers can be probed, which in turn give information regarding the molecular processes through which energy is generated in objects (see Audouze, 1977).

1.2 Significance of Nitric Oxide

Nitric oxide is a very interesting molecule because in its ground electronic state it has an unpaired π electron which gives rise to the $X^2\Pi$ state with $X^2\Pi_{1/2}$ and $X^2\Pi_{3/2}$ components separated by about 120 cm^{-1} due to spin-orbit interaction. It is a very important active molecule in several regions of the earth's atmosphere. In the atmosphere, where its volume mixing ratio is of the order of $10^{-9} - 10^{-8}$, NO is chiefly produced through oxidation of N_2O by the excited oxygen atom $\text{O}(^1\text{D})$. The N_2O is a by-product of microbial metabolism and is present in relatively large concentrations

in the atmosphere. Other sources of NO in the earth's atmosphere are high altitude aircraft, nuclear blasts, volcanoes, lightning, etc. (McDermid *et al.*, 1982). The role played by various oxides of nitrogen in the catalytic destruction of ozone (O_3) can be understood by the following chemical processes:



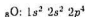
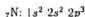
However, nitric oxide in the stratosphere can also be involved in smog reactions and produce ozone. In the troposphere, NO is involved in the photochemical production of ozone and is a major product of internal combustion engines and combustion power plants (Kivel *et al.*, 1957). Global measurements of the NO concentrations in the atmosphere would enhance the understanding of atmospheric physics and chemistry.

The γ ($A^2\Sigma^- - X^2\Pi_r$) system of nitric oxide has important applications in atmosphere science. For example, the bands of this system are used to measure NO column densities in the mesosphere in order to interpret emissions in aurora and to establish the relative spectral response of monochromators in the ultraviolet region (Langhoff *et al.* 1988). Recently, this system has been found to be potentially attractive for an optically-pumped ultraviolet laser with inherently narrow linewidths, since its $A^2\Sigma^+$ state possesses a radiative lifetime of nearly 200 ns and the stimulated $A \rightarrow X$ emission cross section is of the order of 10^{-16} cm^2 (Burrows *et al.* 1985).

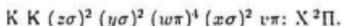
Information from the spectra of nitric oxide has applications in problems concerning the upper atmosphere, pollution, hot air re-entry into the atmosphere, and combustion. In these applications, quantitative data on wavelengths, absorption coefficients, oscillator strengths f , etc., are needed. However, interest in the electronically excited states of NO stems from the theory of molecular structure and quantum mechanics.

1.3 Electronic Configurations and Potential Energy Curves of NO

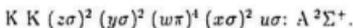
The ground state electronic configurations of the nitrogen and oxygen atoms are



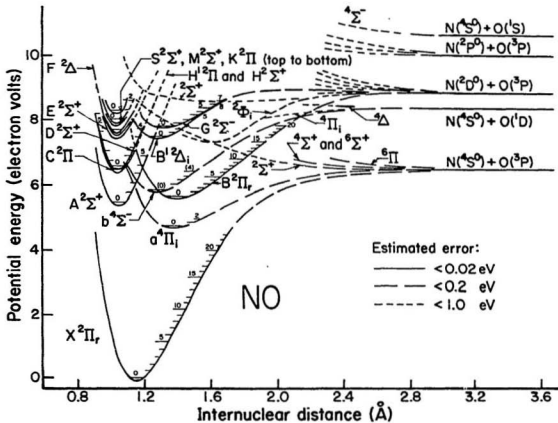
The electrons in the outermost shells of the constituent atoms of a molecule determine the molecular binding and the nature of the molecular states. The electronic configuration which gives rise to the ground state ($X^2\Pi$) of the NO molecule is expressed as:



The first excited doublet $A^2\Sigma^+$ state of NO is obtained by taking the antibonding $v\pi$ electron to the $u\sigma$ Rydberg orbital as shown below:



The γ system arises from the transition $A^2\Sigma^+ - X^2\Pi$. Gilmore (1965) has given potential energy curves for N_2 , NO and O_2 and their ions N_2^+ , NO^+ and O_2^+ . The potential energy curves of the electronic states of NO adopted from Gilmore are shown in Figure 1.1.

Figure 1.1 Potential energy curve for the electronic states of $^{14}\text{N } ^{16}\text{O}$ as modified from Gilmore, 1961.

1.4 Previous Work on the γ ($A^2\Sigma^+ - X^2\Pi$) System and the Infrared Vibration-Rotation and Pure Rotation Spectra in the $X^2\Pi$ state of Nitric Oxide

Because of the importance of the nitric oxide molecule, the spectra of the most abundant isotopomer $^{14}\text{N}^{16}\text{O}$ have been studied by many investigations over a long period. Strutt (1917) was the first to observe the γ system of NO. Subsequently numerous investigations have been carried out on different types of spectra of NO, which include the electronic spectra, vibration-rotation spectra, pure rotation spectra, rotational Raman spectra, magnetic rotation spectra, magnetic and electronic spectra, etc. For references on these earlier studies the reader is referred to a review article by Miescher and Huber (1976) and Huber and Herzberg (1979). "Berkeley News Letters" are to be consulted for more recent references on this subject. We review briefly here the work done since 1970 on the γ ($A^2\Sigma^+ - X^2\Pi$) system and the Infrared and microwave spectra of the isotopomer $^{14}\text{N}^{16}\text{O}$, $^{14}\text{N}^{18}\text{O}$, $^{15}\text{N}^{18}\text{O}$, $^{15}\text{N}^{16}\text{O}$ and $^{15}\text{N}^{17}\text{O}$, arising from the ground state $X^2\Pi_r$.

Cisak *et al.* (1970) measured part of the γ system of $^{15}\text{N}^{16}\text{O}$ and $^{14}\text{N}^{16}\text{O}$ under medium resolution of a quartz prism spectrograph and obtained the vibrational constants and isotopic displacements. Engleman Jr. *et al.* (1970) studied the 1-0 band of the γ system of $^{15}\text{N}^{16}\text{O}$ and $^{14}\text{N}^{18}\text{O}$ (in addition some bands of $^{14}\text{N}^{16}\text{O}$). Engleman Jr. and Rouse (1971) studied 17 bands of $^{14}\text{N}^{16}\text{O}$ γ system in the spectral region 2700 -3100 Å under high resolution and determined the molecular constants for $v=0$ to 16 of the $X^2\Pi$ state and $v=0$ to 5 of the $A^2\Sigma^+$ state. Freedman and Nicholls (1980) reanalyzed the high resolution data of the 1-0 and 0-0 bands of the γ system of $^{14}\text{N}^{16}\text{O}$ and the 1-2 band of $^{14}\text{N}^{18}\text{O}$ and $^{15}\text{N}^{16}\text{O}$, obtained by Engleman

Jr. and Rouse (1971), using the unique perturber treatment methods described by Zare *et al.* (1973).

Amiot *et al.* (1978) obtained the high resolution Fourier spectra of the infrared vibration bands 1-0 and 2-0 of $^{14}\text{N}^{16}\text{O}$ and 1-0 band of $^{14}\text{N}^{17}\text{O}$, $^{14}\text{N}^{18}\text{O}$ and $^{15}\text{N}^{16}\text{O}$ in the $X^2\Pi$ state. These authors reported a detailed analysis of the 1-0 band of $^{14}\text{N}^{16}\text{O}$ and the preliminary results for the spectra of the other isotopomers. Amiot and Guelachvili (1979) investigated similar spectra of the 1-0 and 2-1 bands of $^{15}\text{N}^{16}\text{O}$ and the 1-0 band of $^{15}\text{N}^{17}\text{O}$ and $^{15}\text{N}^{18}\text{O}$ in the $X^2\Pi$ state. Molecular constants of these isotopomers were determined by these authors using the direct approach method.

The analysis of the infrared 1-0, 2-0 and 3-0 bands of $^{14}\text{N}^{16}\text{O}$ in the $X^2\Pi$ state was reported by Valentin *et al.* (1978) and Henry *et al.* (1978). Teffo *et al.* (1980) reported the results of the analysis of the infrared vibration-rotation 1-0, 2-0 and 3-0 bands and the $X^2\Pi_{3/2} - ^2\Pi_{1/2}(1-0)$ subband of $^{15}\text{N}^{16}\text{O}$ and $^{15}\text{N}^{18}\text{O}$.

Molecular beam technique was used by Meerts and Dymanus (1972) to obtain extremely precise Λ doubling and hyperfine structure constants of $^{14}\text{N}^{16}\text{O}$. Patel and Kerl (1978) used the opto-acoustic spectroscopy for the study of $^{14}\text{N}^{16}\text{O}$ and obtained accurate values of the Λ doubling for the $^2\Pi_{1/2} v=0$ and 1 levels. High resolution laser magnetic resonance and infrared-radio-frequency double-resonance spectra of the 1-0 and 2-1 bands of $^{14}\text{N}^{16}\text{O}$, $^{15}\text{N}^{16}\text{O}$, $^{14}\text{N}^{18}\text{O}$ and $^{14}\text{N}^{17}\text{O}$ in the $X^2\Pi$ state have been studied by Dale *et al.* (1977).

1.5 Present work

The present research project is concerned about the observation of the vibrational spectra of the γ ($A^2\Sigma^- - X^2\Pi_r$) system of the nitric oxide isotopomers $^{14}\text{N}^{16}\text{O}$, $^{15}\text{N}^{16}\text{O}$, $^{14}\text{N}^{18}\text{O}$ and $^{15}\text{N}^{18}\text{O}$ under medium dispersion and its analysis. Also, it is the aim of the present work to record this system of $^{15}\text{N}^{18}\text{O}$ under high resolution and to carry out the rotational analysis of several bands. The γ system of NO was excited in the anode glow of a two-column hollow-cathode discharge tube, designed in our laboratory, and photographed in the spectral region 2140-2730 Å under medium resolution of a 2 m Bausch and Lomb spectrograph. The vibrational analysis of the band heads of this system for each of the isotopomers was carried out and the vibrational constants of the upper and lower electronic states A and X were determined. The spectrum of the γ system of $^{15}\text{N}^{18}\text{O}$ has been observed for the first time. The 0-1, 0-2 and 0-3 bands of this isotopomer were photographed under the high resolution on a 3.4 m Jarrell-Ash spectrograph in the fifth order of a 1200 grooves/mm grating. The rotational structure of these bands has been analyzed using the effective Hamiltonian method and a unique set of molecular constants for the A and X states of $^{15}\text{N}^{18}\text{O}$ was obtained.

Chapter 2 describes the experimental techniques. Theoretical aspects of the NO γ system are presented in Chapter 3. Details of the vibrational and rotational analyses of this system of the isotopomers of NO are given in Chapter 4.

Chapter 2

EXPERIMENTAL TECHNIQUES

The nitric-oxide isotopomers $^{14}\text{N}^{16}\text{O}$, $^{15}\text{N}^{16}\text{O}$, $^{14}\text{N}^{18}\text{O}$ and $^{15}\text{N}^{18}\text{O}$ were excited in a two-column hollow-cathode discharge tube. The gamma (γ) ($A^2\Sigma^+ - X^2\Pi_r$) system of these isotopomers resulting from this excitation was photographed with medium and high resolution optical spectrographs. A concise description of the spectrographs, the discharge tube and the experimental procedure is given in this chapter.

2.1 Two-Column Hollow-Cathode Discharge Tube

A schematic diagram of the design of the two-column hollow-cathode discharge tube and the gas-handling system is shown in Figure 2.1. The discharge tube consists of a copper hollow cathode C, a Kovar-Pyrex seal K, a Pyrex glass body S, a tungsten anode A, a cathode window W_1 and an anode window W_2 . The hollow-cathode (9.0 cm long, 1.8 cm in outer diameter and 0.1 cm in wall thickness) was silver-soldered to the Kovar tube (1.9 cm in inner diameter). The Pyrex section of the Kovar-Pyrex seal is joined to the main Pyrex glass body (14 cm long and 4.6 cm in outer diameter). A side-arm (1.7 cm in outer diameter) branches off from the main body of the discharge tube. A tungsten anode was fused into the branch of the side arm. The quartz windows W_1 and W_2 of S1-UV type, supplied by Esco

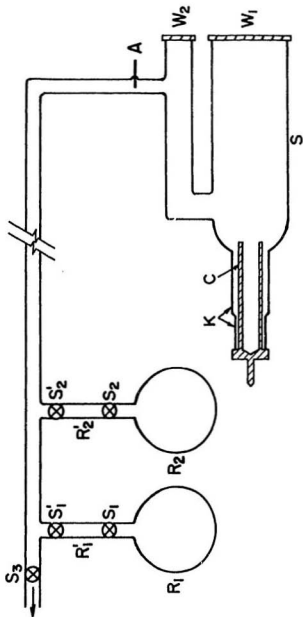


Figure 2.1 A schematic diagram of the hollow-cathode discharge tube and the gas-handling system. Reservoir R_1 and R_2 contain $^{16}\text{O}_2$ and $^{15}\text{N}_2$ gas, respectively; S_1 , S'_1 , S_2 , and S'_2 stop cocks; C : copper hollow-cathode; S : pyrex glass body; A : tungsten anode; W_1 and W_2 : quartz windows; K : kovar; pyrex seal.

Products Inc., are 0.3 cm thick and were attached to the ground end surfaces of the cathode and anode branches of the discharge tube with Torr Seal (which is a low vapor pressure resin). In Figure 2.1, R_1 and R_2 are the reservoirs for oxygen-18 and nitrogen-15, respectively, and R'_1 and R'_2 are the corresponding secondary reservoirs.

The hollow-cathode discharge tube's main advantage is the physical separation of the cathode and anode glows which can be independently photographed. The cathode glow is an excellent source for the molecular ions and the anode glow is a convenient source for the neutral molecules. Reddy and Prasad (1989) have given details of this discharge tube with examples of excitation of the spectra of the molecular ions CO^+ , CO_2^+ and N_2^+ in the cathode emission and those of neutral molecules CO and N_2 in the anode emission.

In the excitation of certain molecular ions, it is sometimes necessary to use, in addition to the experimental substance, a carrier gas such as helium or neon. When high current is required for the excitation of the spectra, it may be necessary to cool the cathode with running cold water or to immerse the cathode portion in a coolant such as liquid nitrogen. In the present experiments, for the excitation of the spectra of the isotopomers of NO, neither a carrier gas nor a coolant was found necessary. In the present study the γ system of NO is excited in the anode column of the discharge tube.

A D.C. power supply unit rated at 2000 V and 250 mA was used to maintain the discharge. The circuit diagram of this unit is shown in Figure 2.2. It consists of a powerstat P, a step-up transformer T (1750-0-1750 V), a bridge rectifier with four high voltage diffused silicon rectifiers D_1 to D_4 (VARO VC40), an oil filled capacitor ($15 \mu F$, 2000 V) and several Dale HL100 type resistors R_1 to R_7 (R_1 : 100 Ω , 100 W; R_2 : 1 to 20 k Ω , 100 W; R_3 to R_4 : 20 k Ω , 100 W; R_5 : 390 k Ω , 9 W). The output voltage is controlled by adjusting the primary voltage of the transformer. In the present experiments the output voltage and current are 1100 V and 70 mA, respectively.

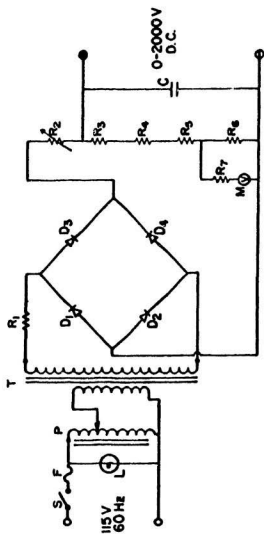


Figure 2.2 Circuit diagram for the 2000 V d.c. power supply unit. T: step-up transformer; R₁ to R₈: resistors; P: powerstat; C: oil-filled capacitor; D₁ to D₄: rectifiers; M: voltmeter.

2.2 Mechanism of a Hollow-Cathode Discharge

When a d.c. voltage is applied between the cathode and the anode of a discharge tube, electrons released and accelerated from the cathode collide with the molecules (or atoms) of the experimental gas and excite them to higher energy states and ionize some of them. The excited positive molecular ions concentrate around the cathode while the neutral molecules spread out in the discharge tube. In the present design, the provision of separate columns for the cathode and anode glows facilitates recording the radiations from these two columns independently. The molecules or their ions excited to different higher unstable rotational, vibrational and electronic states return to the lower energy states by emitting electromagnetic radiation of energy $h\nu'$, h being the Planck's constant and ν' being the frequency (in s^{-1}) of the emitted photon. As long as the discharge is maintained between two electrodes, collisions between the electrons and the molecules (or the atoms) continue to take place and the emission of radiation is maintained. One of the advantages of a hollow cathode discharge tube relative to a parallel plate d.c. discharge is that the temperature of the hollow-cathode is lower than that of the cathode plate under similar excitation conditions. Because of this the spectral lines from the hollow-cathode discharge tube have smaller Doppler widths. Another advantage is that the discharge is steady in the former case. Also, in a hollow-cathode discharge tube, the effects of pressure broadening and Stark broadening of spectral lines are minimized.

2.3 Spectrographs

A 2 m Bausch and Lomb dual grating spectrograph and a 3.4 m Jarrell-Ash Ebert grating spectrograph are used to record the electronic spectra of NO. A brief description of the spectrographs and the experimental procedure is given below.

(a) The 2 m Bausch and Lomb Dual Grating Spectrograph

The optical layout of the 2 m Bausch and Lomb dual grating spectrograph is schematically shown in Figure 2.3 for an incident monochromatic light beam. The light beam which is collimated onto the adjustable slit S is reflected by the plane mirror M onto the upper section of the spherical mirror CM which has a focal length of 2 m and a numerical aperture of $f/15.5$. The reflected light is dispersed by one of the gratings G_1 which has 600 grooves/mm and is blazed at $2.5 \mu\text{m}$ or G_2 which has 1200 grooves/mm and is blazed at $1.0 \mu\text{m}$. These plane gratings, each with a ruled area of 128 mm (width) \times 102 mm (length) are mounted back to back on a rotatable turret T. The dispersed light reaches the lower part of the spherical mirror which focuses the light onto the photographic plate P. The plate holder can accommodate one 10 15 cm \times 25.40 cm plate or two 5.08 cm \times 25.40 cm photographic plates. The measured reciprocal dispersions of the spectra are 4.14 $\text{\AA}/\text{mm}$ at 2157 \AA in the first order of the 600 grooves/mm grating, and 2.01 $\text{\AA}/\text{mm}$ at 2367 \AA in the first order of 1200 grooves/mm grating.



Figure 2.3 Optical layout of the 2 m Bausch and Lomb grating spectrograph with a monochromatic light beam; S': virtual position of S; P: photographic plate; CM: collimating mirror; S: slit; T: rotatable turret; G₁ and G₂: gratings; M: plane mirror.

(b) The 3.4 m Jarrell-Ash Ebert Grating Spectrograph

The optical layout of the 3.4 m Jarrell-Ash spectrograph is schematically shown in Figure 2.4 for polychromatic incident light. This is similar to that of the 2 m Bausch and Lomb spectrograph except that the slit and the plate holder are on the same side for the 3.4 m instrument. Light from the source, after passing through two quartz cylindrical lenses L_1 (10.0 cm in focal length and 3.0 cm in diameter), and L_2 (45.0 cm in focal length and 3.0 cm in diameter), is incident directly on the upper section of the concave mirror M (radius of curvature: 6.655 m, diameter: 40.6 cm and numerical aperture: $f/35$). It is then collimated onto the grating G by mirror M . The dispersed light from the grating is focused onto the photographic plate P by the lower section of M . The plate holder which holds the photographic plates can be tilted about a vertical axis. For a fixed slit position, obtained for the best focus condition, the tilt of the plate holder has a linear dependence on the grating angle. A typical plot of the plateholder tilt versus grating angle for this spectrograph is given by Prasad(1987). An MIT echelle grating having 300 grooves/mm and blazed at $5.7 \mu\text{m}$ and a Bausch and Lomb plane grating having 1200 grooves/mm and blazed at $1.4 \mu\text{m}$ are available for this spectrograph. The ruled area of each of these gratings is 186 mm (width) \times 63 mm (length). In the present work the 1200 grooves/mm grating was used in the fourth order for the standard spectral lines and in fifth order for the ^{15}N ^{18}O spectrum. The measured reciprocal dispersions of the spectra are $0.343 \text{ \AA}/\text{mm}$ at 2455 \AA in the fifth order.

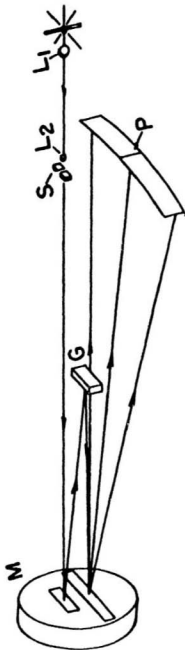


Figure 2.4 Optical layout of the 3.4 m Jarrell-Ash Ebert grating spectrograph with a polychromatic light beam. G: grating; P: photographic plate; M: collimating mirror; S: slit; L₁: quartz cylindrical source lens; L₂: quartz cylindrical slit lens.

2.4 Experimental Procedure

The experimental gases nitrogen-15 and oxygen-18, with specified purities of 99.9% and 98% respectively, were used in the present work. The gas-handling system made of Pyrex glass which was connected to the hollow-cathode discharge tube is shown schematically in Figure 2.1.

Reservoirs R_1 and R_2 contain $^{18}\text{O}_2$ and $^{15}\text{N}_2$ respectively. R'_1 and R'_2 represent the secondary reservoirs for these gases. With the stop cocks S_1 and S_2 in closed position, the whole gas handling system and the discharge tube were thoroughly evacuated. The secondary reservoirs R'_1 and R'_2 were then filled with $^{18}\text{O}_2$ and $^{15}\text{N}_2$, respectively. With stop cock S_3 in closed position, small amounts of $^{18}\text{O}_2$ and $^{15}\text{N}_2$ were admitted into the discharge tube through S'_1 and S'_2 , respectively. An approximate ratio of $^{18}\text{O}_2$ to $^{15}\text{N}_2$ admitted into the discharge tube is $\sim 2:1$ for the excitation of the $^{15}\text{N}^{18}\text{O}$ spectrum. When only $^{15}\text{N}_2$ was admitted in the discharge tube, the spectrum of $^{15}\text{N}^{16}\text{O}$ was excited. If only $^{18}\text{O}_2$ was admitted, the spectrum of $^{14}\text{N}^{18}\text{O}$ was excited. However, the spectrum of $^{14}\text{N}^{16}\text{O}$ was obtained by the natural presence of $^{16}\text{O}_2$ and $^{14}\text{N}_2$ of low pressure air in the discharge tube. The pressure in the discharge tube for the best excitation condition is approximately 0.8 Torr.

A DC voltage of 1100 V is applied between the electrodes of the discharge tube. A Tesla coil was used to initiate the discharge. The pressure of the gas inside the discharge tube was regulated until a bright and steady discharge was obtained. The

medium resolution emission spectra of $^{15}\text{N}^{18}\text{O}$, $^{15}\text{N}^{16}\text{O}$, $^{14}\text{N}^{18}\text{O}$ and $^{14}\text{N}^{16}\text{O}$ in region 2140-2730 Å were photographed on the Bausch and Lomb spectrograph and the high resolution emission spectra in the same region were photographed on the Jarrell-Ash spectrograph. The slit width was set at 20 μm for the former and 25 μm for the latter. Iron arc and copper arc, both of d.c. type, were used as the sources of the standard spectra recorded on the Bausch and Lomb spectrograph. An iron-neon hollow-cathode lamp was used as the standard source for the high resolution spectra recorded on the Jarrell-Ash instrument. The axis of the hollow-cathode discharge tube and the axis of the Jarrell-Ash spectrograph coincide with each other, and the axis of the Fe-Ne lamp is perpendicular to the axis of the spectrograph. A front-surface-coated plane mirror, mounted on an optical bench, reflects the light from the Fe-Ne lamp onto the slit of the spectrograph. It can be moved from and reset in the original position on the optical bench, thus ensuring best collimation condition.

A Hoya U-340 glass filter and a chlorine gas filter were used to eliminate the overlapping orders. Kodak SWR photographic plates were used to record the spectra. The exposure times varied from 3 seconds to 4.5 hours, depending on the intensity of the band, order of the grating, and the type of filter. The photographic plates were developed in Kodak developer D-19 at room temperature for about 4 minutes and were then fixed in Kodak fixer for 30 minutes.

2.5 Measurement of Spectra

The spectra were measured on a model M 1205C comparator, supplied by Gaertner

Optical Co.. Although the least count of this instrument is 0.001 mm, the reading can be estimated to an accuracy of 0.0005 mm. The relation between air wavelengths λ_{air} of the spectral lines and their comparator readings d is given by the following polynomial equation

$$\lambda_{\text{air}} = \sum_{i=0}^n a_i (d - d_0)^i, \quad (2.1)$$

where d_0 is the comparator reading of the first standard line and a_i are the coefficients of the polynomial. The method of least squares fitting was used to obtain the values of these coefficients from the wavelengths of standard lines. In general the standard deviations of the fit were about 0.012 Å and 0.003 Å for medium and high resolution spectrum, respectively. The wavelengths of the standard Fe-arc lines and Cu-arc lines were taken from Gatterer and Junkes (1956) and Shenstone (1955) respectively, and the standard Fe-Nc lines from Crosswhite (1958 and 1975). The air wavelengths of the band heads and the rotational lines were then calculated using the values of a_i . The following Edlen's formula (1953) for the refractive index n was used to convert the air wavelengths into vacuum wavenumbers:

$$n = 1 + 6432.8 \times 10^{-8} + \frac{2949810}{146 \times 10^8 - \nu^2} + \frac{25540}{41 \times 10^8 - \nu^2}, \quad (2.2)$$

where $\nu = 10^8 / (n\lambda_{\text{air}})$, and λ_{air} are in Ångström units. An iterative method was used until the absolute value of the difference between the successive values of the wavenumbers was less than or equal to 10^{-10} cm^{-1} . The analysis of the spectra was performed on Vax 11/785 and Unix Dec System 5500 computers.

Chapter 3

THEORETICAL ASPECTS FOR THE ANALYSIS OF THE NO γ SYSTEM

In this chapter the theoretical aspects of the electronic spectra of diatomic molecules which are relevant to the present work are described. A detailed theory of the electronic band spectra is found in Mulliken (1931, 1932) and Herzberg (1950, 1971).

3.1 Vibrational and Rotational Structures of Electronic Band Systems

(i) Electronic and vibrational terms

The total energy E (usually expressed in ergs) of a diatomic molecule is represented as the sum of its electronic energy E_e , vibrational energy E_v and rotational energy E_r (within the Born-Oppenheimer approximation). Accordingly

$$E = E_e + E_v + E_r. \quad (3.1)$$

In this treatment the translational and nuclear spin energies are excluded from consideration. The term value T (in cm^{-1}) of an energy level is represented by

$$T = E/hc = T_e + G(v) + F_v(J), \quad (3.2)$$

where v and J are the vibrational and rotational quantum numbers respectively, and T_e , $G(v)$ and $F_v(J)$ are the electronic, vibrational and rotational terms, respectively.

The wavenumber (in cm^{-1}) of a spectral line between the rotational levels of an upper ($'$) and a lower ($''$) electronic state is given by

$$\begin{aligned}\nu &= T' - T'' \\ &= (T'_e - T''_e) + [G'(v') - G''(v'')] + [F'_v(J') - F''_v(J'')] \\ &= \nu_e + \nu_v + \nu_r.\end{aligned}\tag{3.3}$$

For a given electronic transition, $\nu_e = T'_e - T''_e$ is the system origin and $\nu_e + \nu_v = \nu_0$ is the band origin, where $\nu_v = G'(v') - G''(v'')$ and $\nu_r = F'_v(J') - F''_v(J'')$.

The electronic terms for different multiplet components of an electronic state are generally expressed in the first approximation, *i.e.*, considering no rotation and vibration of the molecule, as

$$T_e = T_0 + A\Lambda\Sigma_s,\tag{3.4}$$

where T_0 is the electronic term, neglecting the electronic spin, Λ and Σ_s are the quantized projections along the internuclear axis of the electron orbital angular momentum \vec{L} and the electron spin angular momentum \vec{S} , respectively, and A is the spin-orbit coupling constant. The electronic states are labelled Σ , Π , Δ , $\Phi \dots$ for $\Lambda = 0, 1, 2, 3, \dots$, respectively. For a regular state, (*eg.* Π_r state), A is positive, and for inverted state, (*eg.* Π_i state) A is negative. Depending on whether the electronic wave function ψ_e remains unchanged or changes sign when reflected at any plane passing through the internuclear axis, the electronic $\Sigma(\Lambda = 0)$ states are designated as Σ^+ or Σ^- . The multiplicity of an electronic state is given by $2S + 1$, which is the number of components of \vec{S} projected along the internuclear axis.

The vibrational terms $G(v)$ of an electronic state of a molecule are expressed as

$$G(v) = \omega_e(v + 1/2) - \omega_e x_e(v + 1/2)^2 + \omega_e y_e(v + 1/2)^3 + \dots, \quad (3.5)$$

where ω_e (in cm^{-1}) is the vibrational constant and $\omega_e x_e$, $\omega_e y_e$, etc., (also in cm^{-1}) represent the anharmonic terms of the vibrational motion.

(ii) Vibrational structure of the electronic spectra and the isotope shifts

The wavenumber $\nu_{v',v''}$ of a vibrational transition, neglecting the contribution from the rotational levels is given by

$$\begin{aligned} \nu_{v',v''} = & \nu_0 + \omega_e'(v' + 1/2) - \omega_e' x_e'(v' + 1/2)^2 + \omega_e' y_e'(v' + 1/2)^3 + \dots \\ & - \omega_e''(v'' + 1/2) + \omega_e'' x_e''(v'' + 1/2)^2 - \omega_e'' y_e''(v'' + 1/2)^3 + \dots \end{aligned} \quad (3.6)$$

If detailed rotational analysis of the structure of many bands of an electronic band system is carried out, the band origins ν_0 can be directly fitted to Equation 3.6 and the constants ν_0 , ω_e , $\omega_e x_e$, $\omega_e y_e$, etc., are obtained. In the absence of such an analysis, the wavenumbers of the band heads are fitted to the above equation to obtain the specified constants.

The vibrational isotope shift $\Delta\nu$ of a band with given v' and v'' is represented by

$$\begin{aligned} \Delta\nu = & \nu_{v',v''} - \nu_{v',v''}^i \\ = & (1 - \rho)[\omega_e'(v' + 1/2) - \omega_e''(v'' + 1/2)] \\ & - (1 - \rho^2)[\omega_e' x_e'(v' + 1/2)^2 - \omega_e'' x_e''(v'' + 1/2)^2] \\ & + (1 - \rho^3)[\omega_e' y_e'(v' + 1/2)^3 - \omega_e'' y_e''(v'' + 1/2)^3] + \dots, \end{aligned} \quad (3.7)$$

where $\nu_{v',v''}$ and $\nu_{v',v''}^i$ are the wavenumbers of the band origins (or band heads), with given v' and v'' of an ordinary molecule and its isotope, respectively, and $\rho = [\mu/\mu^i]^{1/2}$.

Here μ and μ' are the reduced masses of these molecules ($\mu=(m_1 m_2)/(m_1 + m_2)$).

(iii) Coupling between rotational and electronic motions

The splitting of the rotational levels in these multiplet states depends on the type of coupling between various angular momenta of the molecule. Hund's case (a) and case (b), which are important for the present work, will be discussed here. In Hund's case (a), we come across spin-orbit coupling and Λ -type doubling.

Spin-orbit coupling: The interaction of the spin angular momentum of the electrons with their orbital angular momentum causes splitting in the electronic states. In Hund's case (a) the coupling of the nuclear rotation angular momentum \vec{R} with electronic motion is weak, and the electronic orbital and spin angular momenta \vec{L} and \vec{S} are strongly coupled individually to the internuclear axis. The sum of the quantized projections along the internuclear axis of the electron orbital and the spin angular momenta is given as

$$\Omega = \Lambda + \Sigma_s. \quad (3.8)$$

The electronic states Σ , Π , Δ , Φ , etc., have $\Lambda=0, 1, 2, 3,$ etc., respectively. For a fixed Λ , Ω can take $2S+1$ values. Thus the components arising from the spin-orbit coupling of a ${}^2\Pi$ state are ${}^2\Pi_{3/2}$ and ${}^2\Pi_{1/2}$. In Hund's case (a), \vec{R} and $\vec{\Omega}$ combine to form the total angular momentum \vec{J} . For a given value Ω , quantum number J is given by

$$J = \Omega, \Omega + 1, \Omega + 2 \dots \quad (3.9)$$

Both J and Ω have either integer or half integer values depending on whether the multiplicity ($2S+1$) of the state is odd or even, respectively.

Λ -type doubling: Even though the coupling between the rotation of a molecule and the orbital motion of its electrons is very small, it gives rise to a splitting of the degeneracy that arises for the electronic states with $\Lambda \neq 0$. This splitting is called Λ -type doubling.

In Hund's case (b) the spin vector \vec{S} is weakly coupled to the internuclear axis (this means that $\vec{\Omega}$ is not defined) and \vec{L} combines with \vec{R} to form the new vector \vec{N} , which is the total angular momentum apart from the spin. The quantum number N is given by

$$N = \Lambda, \Lambda + 1, \Lambda + 2, \dots \quad (3.10)$$

The vector \vec{N} combines with \vec{S} to form \vec{J} . For a given N , J has the values

$$J = N + S, N + S - 1, N + S - 2, \dots, |N - S|. \quad (3.11)$$

Thus each rotational level N has $(2S+1)$ components (which represent the multiplicity of the states). In this case, J can be either an integer or a half-integer, depending on the multiplicity being odd or even. Σ states always belong to Hund's case (b); and multiplet Π , Δ , etc., states can belong to Hund's case (a) or Hund's case (b).

Hund's coupling cases represent idealized limiting cases. They represent the observed spectra to a good approximation. However, small or even large deviations from these limiting cases are found. The reason for this is that some interactions were neglected in the idealized coupling cases, and particularly that the relative magnitude of the interactions changes with increasing rotation. Thus, a transition takes place from one coupling case to another with increasing rotation. For the $X^2\Pi$ state of

NO, a transition takes place from case (a) to case (b) at high J values.

A rotational level is positive or negative depending upon whether the total eigenfunction (Ψ) remains unchanged or changes sign upon reflection at the origin. This property is called the parity. Kopp and Hougen (1967) introduced the following convention for labeling the rotational levels with half integer J values:

“levels with parity $[+(-1)^{J-1/2}]$ are e levels
and those with parity $[-(-1)^{J-1/2}]$ are f levels.”

Later Brown *et al.* (1975) extended this labeling convention to the rotational levels with integer J values as

“levels with parity $[+(-1)^J]$ are e levels
and those with parity $[-(-1)^J]$ are f levels.”

(iv) Rotational terms of the electronic states

The rotational terms of a given vibrational level of a singlet electronic state are represented by

$$F_v(J) = B_v[J(J+1) - \Lambda^2] - D_v[J(J+1) - \Lambda^2]^2 + \dots, \quad (3.12)$$

and those of a multiplet electronic state belonging to Hund's case (a) are given by

$$F_v(J) = B_v[J(J+1) - \Omega^2] - D_v[J(J+1) - \Omega^2]^2 + \dots, \quad (3.13)$$

where B_v and D_v are rotational and centrifugal distortion constants, respectively. These constants can be expressed in terms of the vibrational quantum number v and

the equilibrium molecular constants B_v , α_e , γ_e , D_e and β_e as

$$B_v = B_e - \alpha_e(v + 1/2) + \gamma_e(v + 1/2)^2 + \dots, \quad (3.14)$$

and

$$D_v = D_e + \beta_e(v + 1/2), \quad (3.15)$$

where $B_e = h/(8\pi c\mu r_e^2)$, and $D_e = 4B_e^3/\omega_e^2$ (Kratzer's relation). r_e represents the equilibrium internuclear distance and μ is the reduced mass. Here $\alpha_e \ll B_e$, $\beta_e \ll D_e$ and $\gamma_e \ll \alpha_e$. Here h and c are universal constants.

The rotational levels of a ${}^2\Sigma^+$ state in Hund's case (b) are given by

$$F_{1e}(N) = B_v N(N+1) - D_v N^2(N+1)^2 + \frac{1}{2}\gamma_v N, \quad (3.16)$$

$$F_{2f}(N) = B_v N(N+1) - D_v N^2(N+1)^2 - \frac{1}{2}\gamma_v(N+1), \quad (3.17)$$

where $F_{1e}(N)$ and $F_{2f}(N)$ refer to the components with $J=N+1/2$ and $N-1/2$, respectively, and γ_v is the spin-splitting constants (also called spin-rotation interaction constant). In terms of J , $F_{1e}(N)$ and $F_{2f}(N)$ can be written as

$$F_{1e}(J) = B_v(J-1/2)(J+1/2) - D_v(J-1/2)^2(J+1/2)^2 + \frac{1}{2}\gamma_v(J-1/2), \quad (3.18)$$

and

$$F_{2f}(J) = B_v(J+1/2)(J+3/2) - D_v(J+1/2)^2(J+3/2)^2 - \frac{1}{2}\gamma_v(J+3/2). \quad (3.19)$$

In a ${}^2\Pi_r$ state, a series of rotational levels exists for each of the sub-states ${}^2\Pi_{1/2}$ and ${}^2\Pi_{3/2}$ with the levels of ${}^2\Pi_{3/2}$ having higher energy than the corresponding levels of ${}^2\Pi_{1/2}$. Hence the ${}^2\Pi_{1/2}$ levels are called the F_1 levels and the other ones are called the F_2 levels. In both ${}^2\Pi_{1/2}$ and ${}^2\Pi_{3/2}$, the rotational levels are doubly degenerate

due to the Λ -doubling. All these four types of rotational levels can be represented by the following expressions:

${}^2\Pi_{1/2}$:

$$\begin{aligned}
 F_{2e}(J) &= B_v[J(J+1) - 1.75] - D_v[J(J+1) - 1.75]^2 \\
 &\quad + \frac{1}{2} \left[\frac{p_v B_v^2}{A_v^2} + \frac{2q_v B_v}{A_v} \right] (1 - 1/2)(J + 1/2)(J + 3/2) \\
 &\quad + \frac{1}{2} A_v + \frac{1}{2} A_{Dv} [J(J+1) - 1.75], \quad (3.20)
 \end{aligned}$$

$$\begin{aligned}
 F_{2f}(J) &= B_v[J(J+1) - 1.75] - D_v[J(J+1) - 1.75]^2 \\
 &\quad - \frac{1}{2} \left[\frac{p_v B_v^2}{A_v^2} + \frac{2q_v B_v}{A_v} \right] (1 - 1/2)(J + 1/2)(J + 3/2) \\
 &\quad + \frac{1}{2} A_v + \frac{1}{2} A_{Dv} [J(J+1) - 1.75], \quad (3.21)
 \end{aligned}$$

${}^2\Pi_{1/2}$:

$$\begin{aligned}
 F_{1e}(J) &= B_v[J(J+1) + 0.25] - D_v[J(J+1) + 0.25]^2 \\
 &\quad + \frac{1}{2} p_v (J + 0.5) - \frac{1}{2} A_v - \frac{1}{2} A_{Dv} [J(J-1) + 0.25], \quad (3.22)
 \end{aligned}$$

$$\begin{aligned}
 F_{1f}(J) &= B_v[J(J+1) + 0.25] - D_v[J(J+1) + 0.25]^2 \\
 &\quad - \frac{1}{2} p_v (J + 0.5) - \frac{1}{2} A_v - \frac{1}{2} A_{Dv} [J(J+1) + 0.25]. \quad (3.23)
 \end{aligned}$$

In the above equations p_v and q_v are the Λ -doubling parameters, A_v is the spin-orbit coupling constant and A_{Dv} is the centrifugal distortion parameter of the spin-orbit coupling constant. The expressions for the twelve branches of the ${}^2\Sigma^+ - {}^2\Pi$ system can be obtained from the general equation

$$\nu = (T_{v\Sigma}'' - T_{v\Pi}'') + F_{\Sigma}''(J') - F_{\Pi}''(J''), \quad (3.24)$$

with $J'' = J$.

3.2 Method of Rotational Analysis

(i) Effective Hamiltonian

In the absence of an external electric or magnetic field, the effective Hamiltonian for a diatomic molecule is expressed as

$$H = H_0 + H_{rot} + H_{cd} + H_{fs} + H_{hfs}, \quad (3.25)$$

where H_0 includes the terms which are independent of rotation and represents the vibronic term energy T_v of different electronic states. The term H_{rot} represents the Hamiltonian describing the rotation of the nuclei, and is given by

$$\begin{aligned} H_{rot} &= B(r)\tilde{R}^2 \\ &= (h/8\pi^2\mu r^2)(\tilde{J} - L' - S')^2, \end{aligned} \quad (3.26)$$

where $B(r)$ is the radial part of the rotational energy operator, μ is the reduced mass, r is the internuclear distance, and \tilde{R} is the rotational angular momentum operator. The term H_{cd} is the Hamiltonian for the centrifugal distortion and is expressed as

$$H_{cd} = -D(\tilde{R}^2)^2 + H(\tilde{R}^2)^3 + \dots, \quad (3.27)$$

where D and H are the quartic and sextic distortion constants. The term H_{fs} describes the fine structure of spectral levels and can be written as

$$H_{fs} = H_{so} + H_{ss} + H_{sr} + H_{ds}, \quad (3.28)$$

where H_{ss} is always equal to zero for the doublet states. The term H_{so} represents the spin-orbit interaction and can be expressed as

$$\begin{aligned} H_{so} &= A(r)\tilde{L} \cdot \tilde{S} + \dots \\ &= A(r)(L_x S_x + 1/2 L_+ S_- + 1/2 L_- S_+) + \dots, \end{aligned} \quad (3.29)$$

where $\Lambda(r)$ is the spin-orbit coupling constant. Equation 3.29 also contains the centrifugal correction terms A_{Dv} , etc. The term H_{sr} in equation 3.28 is the spin-rotation Hamiltonian and is given by

$$\begin{aligned} H_{sr} &= \gamma(r)\vec{R} \cdot \vec{S} \\ &= \gamma(r)(\vec{J} - \vec{L} - \vec{S}) \cdot \vec{S}, \end{aligned} \quad (3.30)$$

where $\gamma(r)$ is the spin-rotation constant, the last term H_{ld} in equation 3.28 is the Λ -doubling in rotational levels and contains the Λ -doubling parameters o , p , q and their centrifugal corrections. This Hamiltonian can be expressed as

$$\begin{aligned} H_{ld} &= o(r)(\Lambda_+^2 S_-^2 + \Lambda_-^2 S_+^2) + p(r)(\Lambda_+^2 S_- N_- + \Lambda_-^2 S_+ N_+) \\ &\quad - q(r)(\Lambda_+^2 N_-^2 + \Lambda_-^2 N_+^2) + \dots \end{aligned} \quad (3.31)$$

The parameter $o(r)$ is zero for multiplicity one or two. The parameters $p(r)$ and $q(r)$ are Λ -doubling parameters for the ${}^2\Pi$ state in this work. The term H_{hfs} in equation 3.25 represents the Hamiltonian for the hyperfine structure, which is too small for optical spectra and can be ignored in the present work.

Brown *et al.* (1979) and later Amiot *et al.* (1981) calculated the corresponding matrix elements of the effective Hamiltonian (equation 3.25) for ${}^2\Sigma^+$ and ${}^2\Pi$ states. Table 3.1 gives the matrix elements of the Hamiltonian for these two states. The measured line positions are compared iteratively with the calculated line positions which are the appropriate differences between the term values of the upper and lower electronic states. These term values are obtained as the eigenvalues of the Hamiltonian matrix.

Table 3.1: Matrix elements of the Hamiltonian for ${}^2\Pi$ and ${}^2\Sigma^+$ states

Molecular constant	Labeling ^a	Matrix element ^{b,c}
T_v	1,1	1
	2,2	1
	3,3	1
B_v	1,1	$x(x \mp 1)$
	2,2	$x^2 - 1$
	3,3	$x^2 + 1$
	2,3	$-(x^2 - 1)^{1/2}$
D_v	1,1	$x^2(x \mp 1)^2$
	2,2	$-x^2(x^2 - 1)$
	3,3	$-x^2(x^2 + 1)$
	2,3	$2x^2(x^2 - 1)^{1/2}$
γ_v	1,1	$0.5(x \mp 1)$
A_v	2,2	0.5
	3,3	-0.5
A_{Dv}	2,2	$0.5(x^2 - 1)$
	3,3	$-0.5(x^2 + 1)$
p_v	3,3	$\mp 0.5x$
q_v	3,3	$\mp x$
	2,3	$\pm 0.5x(x^2 - 1)^{1/2}$

^aLabels 1, 2, and 3 refer to states ${}^2\Sigma^+$, ${}^2\Pi_{3/2}$ and ${}^2\Pi_{1/2}$, respectively.

^b $x = J + 0.5$.

^cThe upper and lower signs of notation \pm and \mp refer to the e and f levels respectively.

In our computer program, the Hamiltonian matrix is diagonalized to obtain the eigenvalues, i.e., the term values of the upper and lower states involved in the transition. The measured line positions are compared iteratively with the calculated line positions which are the appropriate differences between the term values of the two electronic states. The molecular constants are the adjustable parameters in the effective Hamiltonian. An improved set of molecular constants is generated from a least-squares fit of the calculated line positions to the observed ones. This non-linear least-squares procedure is repeated until a set of molecular constants is obtained.

(ii) Method of merging

In the analysis of the data in molecular spectroscopy, multiple estimates of a given molecular parameter are often obtained. A method of "merging" is often used to reduce these multiple estimates to a single "best possible" parameter. Taking into account the uncertainties and the correlations of individual bands, the multiple estimates of the molecular constants are combined together. In the present work, molecular constants obtained from the individual bands using the effective Hamiltonian method of Brown *et al.* (1979), their standard deviations and variance-covariance matrices are used as input parameters for the correlated least-squares merging fit.

The relation between the input parameters and the best possible values of output parameters in the merge procedure is given by the following set of equations in the matrix notation

$$Y = X\beta + \delta, \quad (3.32)$$

where Y , β and δ are the column vectors of the input parameters, the output parameters and the unknown errors, respectively and X is the coefficient matrix. The "best possible" parameters β are obtained in such a way that the squares of the deviations are minimized subject to the inter-relations among δ . An estimate of $\hat{\beta}$ from the least-squares fit in the matrix notation is given by

$$\hat{\beta} = (X^T \Phi^{-1} X)^{-1} X^T \Phi^{-1} Y, \quad (3.33)$$

where Φ is a nondiagonal generalized weight matrix, which is composed of the variance-covariance matrices obtained from the individual band fits. The estimated variance $\hat{\sigma}^2$ is expressed as

$$\hat{\sigma}^2 = (Y - X\hat{\beta})^T \Phi^{-1} (Y - X\hat{\beta}) / f, \quad (3.34)$$

where f is the number of degrees of freedom. The estimated variance-covariance matrix $\hat{\theta}$ which is associated with $\hat{\beta}$ is given by

$$\hat{\theta} = \hat{\sigma}^2 \hat{V}, \quad (3.35)$$

where \hat{V} is the dispersion matrix which can be written as

$$\hat{V} = (X^T \Phi^{-1} X)^{-1}, \quad (3.36)$$

For further details of the method of merging, the reader is referred to Albritton *et al.* (1977), Coxon (1978) and Prasad and Reddy (1988).

3.3 The Rotational Structure of a Band of a ${}^2\Sigma^+ - {}^2\Pi_r$ Transition

A ${}^2\Sigma^+$ state always belongs to Hund's case (b), and the splitting of a ${}^2\Sigma^+$ state is due to the spin splitting. For a ${}^2\Pi$ state, the resultant electron spin S is $1/2$ and

$\Sigma_v = \pm 1/2$, and hence there are two substates ${}^2\Pi_{1/2}$ ($J = 0.5, 1.5 \dots$) and ${}^2\Pi_{3/2}$ ($J = 1.5, 2.5 \dots$). A ${}^2\Pi$ state may belong either to case (a) or case (b) or to cases intermediate between (a) and (b). Since the spin-orbit coupling constant A is large for the $X^2\Pi$ state of NO, the ${}^2\Pi$ state belongs to case (a) at low J values. As the two states ${}^2\Pi$ and ${}^2\Sigma^+$ belong to Hund's case (a) and case (b), respectively, a ${}^2\Sigma^+ - {}^2\Pi$ transition is known as a mixed case transition.

The rotational structure of a band arising from ${}^2\Sigma^+ - {}^2\Pi$ transition consists of twelve branches. The selection rules which govern this transition are as follows:

$$\begin{aligned} \Delta J = 0 & \quad e \longleftrightarrow f \\ \Delta J = \pm 1 & \quad e \longleftrightarrow e, f \longleftrightarrow f \\ & \quad + \longleftrightarrow -, + \longleftrightarrow +, - \longleftrightarrow - \end{aligned}$$

For a regular doublet state, *eg.* ${}^2\Pi_r$ state, the character of the lowest rotational level is “-” and “+”, that is, “-” is for ${}^2\Pi_{1/2}$, and “+” is for ${}^2\Pi_{3/2}$, and the signs are just opposite for a ${}^2\Pi_i$ state (Mulliken, 1931). In accordance with the above selection rules, for each band the following twelve branches occur: R_{21ff} , R_{11ee} , Q_{21fe} , Q_{11ef} , P_{21ff} , P_{11ee} , R_{22ff} , R_{12ee} , Q_{22fe} , Q_{12ef} , P_{22ff} and P_{12ee} . For the γ system of the NO molecule, the four satellite branches Q_{21fe} , P_{21ff} , R_{12ee} and Q_{12ef} are weaker and closer relative to corresponding main branches R_{11ee} , Q_{11ef} , Q_{22fe} , and P_{22ff} , respectively. Thus satellite branches are neither observed nor resolved, therefore in total, eight branches prevail in a band of the ${}^2\Sigma^+ - {}^2\Pi_r$ transitions. In eight-branch bands, the two outer branches R_{21ff} and P_{12ee} are usually decidedly weaker than the other branches (Mulliken 1931).

A schematic energy level diagram including all the twelve branches is shown in Figure 3.1. In this figure, the parity of the levels, selection rules and character of lowest rotational level are taken into consideration as described above.

For the NO γ system, the P_{12er} , P_{22ff}/Q_{12ef} , P_{11re} and Q_{11ef}/P_{21ff} branches form four different heads in the rotational structure of a band. The ${}^2\Sigma^+ - {}^2\Pi_{1/2}$ and ${}^2\Sigma^+ - {}^2\Pi_{3/2}$ subbands have two different band origins. In this work, only the $(T_{v\Sigma} - T_{v\Pi})$ value is determined. The band origins of the two subsystems can be calculated from $(T_{v\Sigma} - T_{v\Pi}) + (1/2)(A_v - 2B_v)$ and $(T_{v\Sigma} - T_{v\Pi}) - (1/2)(A_v - 2B_v)$, respectively.

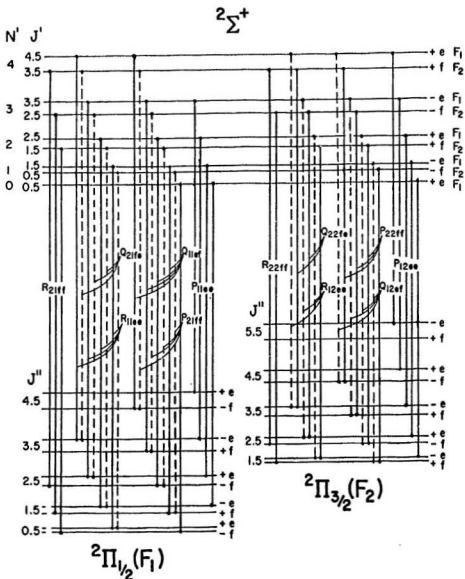


Figure 3.1 A schematic energy level diagram showing the first few rotational transitions of all the twelve branches of a band of a $2\Sigma^+ - 2\Pi$ transition. The dashed lines are satellite branches.

Chapter 4

ANALYSIS OF THE SPECTRA OF THE γ SYSTEM OF NITRIC OXIDE

As mentioned in Chapter 2, the γ system of the nitric oxide isotopomers $^{14}\text{N}^{16}\text{O}$, $^{15}\text{N}^{16}\text{O}$, $^{14}\text{N}^{18}\text{O}$ and $^{15}\text{N}^{18}\text{O}$ were excited in the anode glow of the two-column hollow-cathode discharge tube. Other experimental information is given in detail in the same chapter. Theoretical aspects relevant to the vibrational and rotational analyses presented in this thesis were discussed in Chapter 3. In the present chapter the vibrational and rotational analyses of the γ system of all the four isotopomers are given. Vibrational analysis is presented in Section 4.1 and rotational analysis of the 0-1, 0-2 and 0-3 bands of $^{15}\text{N}^{18}\text{O}$ is given in Section 4.2. Summary of the present research is given in Section 4.3.

4.1 Vibrational Analysis

For each of the isotopomers $^{14}\text{N}^{16}\text{O}$, $^{15}\text{N}^{16}\text{O}$, $^{14}\text{N}^{18}\text{O}$ and $^{15}\text{N}^{18}\text{O}$, the 1-0, 0-0, 0-1, 0-2, 0-3 and 0-4 bands have been observed in the spectral region 2140-2730 Å. The isotopomer $^{14}\text{N}^{16}\text{O}$ was excited with natural presence of nitrogen-14 and oxygen-16 of low pressure air in the discharge tube and the isotopomers $^{15}\text{N}^{16}\text{O}$, $^{14}\text{N}^{18}\text{O}$ and $^{15}\text{N}^{18}\text{O}$ were excited by admitting nitrogen-15, oxygen-18 and a mixture of these, respectively, into the discharge tube. The spectra photographed under the medium dispersion in the first order of a 600 grooves/mm grating on the 2 m Bausch and Lomb

spectrograph are reproduced in Figure 4.1. On account of the known bands of the γ system of $^{14}\text{N}^{16}\text{O}$, the vibrational assignments for the band heads of the other three isotopomers of nitric oxide were found to be straight forward. For each vibrational band, four heads, P_{12ee} and P_{22ff}/Q_{12ef} of $A^2\Sigma^+ - X^2\Pi_{3/2}$ and P_{11ee} and P_{21ff}/Q_{11ef} of $A^2\Sigma^+ - X^2\Pi_{1/2}$ are observed as seen in Figure 4.1. The bands are degraded to shorter wavelengths. The vacuum wavenumbers (in cm^{-1}) of the band heads, their relative intensities and vibrational assignments are listed in Tables 4.1, 4.2, 4.3 and 4.4 for $^{14}\text{N}^{16}\text{O}$, $^{15}\text{N}^{16}\text{O}$, $^{14}\text{N}^{18}\text{O}$ and $^{15}\text{N}^{18}\text{O}$, respectively. The wavenumbers of the band heads are arranged in Deslandres vibrational schemes for these isotopomers in Tables 4.5, 4.6, 4.7 and 4.8, respectively. The vibrational terms $G(v)$ are represented by Equation 3.6 in Chapter 3. If one includes the first anharmonicity term only, $G(v)$ becomes:

$$G(v) = \omega_e(v + 1/2) - \omega_e x_e(v + 1/2)^2. \quad (4.1)$$

The vibrational quanta $\Delta G(v + 1/2)$ between levels v and $v + 1$ of a component of an electronic state are represented by

$$\begin{aligned} \Delta G(v + 1/2) &= G(v + 1) - G(v) \\ &= (\omega_e - \omega_e x_e) - 2\omega_e x_e(v + 1/2). \end{aligned} \quad (4.2)$$

In Deslandres Tables 4.5 to 4.8, the values of $\Delta G(v + 1/2)$ in the upper ($A^2\Sigma^+$) and lower ($X^2\Pi_{1/2}$, $X^2\Pi_{3/2}$) states are also given. The observed vibrational quanta $\Delta G(v + 1/2)$ for the P_{21ff}/Q_{11ef} heads of $X^2\Pi_{1/2}$ and for the P_{22ff}/Q_{12ef} heads of $X^2\Pi_{3/2}$ versus $(v + 1/2)$ are separately fitted to a linear least-squares program and the values of $(\omega_e - \omega_e x_e)$ and $-2\omega_e x_e$ as per Equation 4.2 are obtained. The values of ω_e and $\omega_e x_e$ calculated from these for the two components of the Π state are listed in Table 4.9. For each of the isotopomers, as only the 0 and 1 vibrational levels of the upper $A^2\Sigma^+$ state are observed (from the 0-0 and 1-0 bands), it was possible to obtain

the $\Delta G'(1/2)$ value only. For example, the average value of $\Delta G'(1/2)$ of $\Lambda^2\Sigma^+$ state from the Q heads of $^{14}\text{N}^{16}\text{O}$ is 2345.3 cm^{-1} . Similarly the corresponding $\Delta G'(1/2)$ values are obtained for the other isotopomers and these values are also listed in Table 4.9.

In principle one can calculate the isotope shifts of the vibrational bands in an electronic band system from Equation 3.7. However, these shifts cannot be calculated because only $\Delta G(1/2)$ (not ω_e and $\omega_e x_e$) is known for the $\Lambda^2\Sigma$ state. Instead, the vibrational constants ω_e and $\omega_e x_e$ for the $X^2\Pi_{1/2}$ and $X^2\Pi_{3/2}$ components of $^{15}\text{N}^{16}\text{O}$ and $^{14}\text{N}^{18}\text{O}$ are calculated from those of $^{14}\text{N}^{16}\text{O}$ using the relations

$$\omega_e^i = \rho \omega_e, \quad (4.3)$$

$$\omega_e^i x_e^i = \rho^2 \omega_e x_e, \quad (4.4)$$

where $\rho = (\mu/\mu^i)^{1/2}$, and μ^i is the reduced mass of $^{15}\text{N}^{16}\text{O}$ or $^{14}\text{N}^{18}\text{O}$ ($\rho=0.9821196$ for $^{15}\text{N}^{16}\text{O}$ and $\rho=0.9736636$ for $^{14}\text{N}^{18}\text{O}$). The calculated values of ω_e^i and $\omega_e^i x_e^i$ are also listed in Table 4.9. It is seen from this table that the agreement between the observed and calculated values is very good. If one could use the band origin data instead of the band head data, the agreement would have been even better.

Figure 4.1 Spectra of the γ system of $^{14}\text{N}^{16}\text{O}$, $^{15}\text{N}^{16}\text{O}$, $^{14}\text{N}^{18}\text{O}$, and $^{15}\text{N}^{18}\text{O}$ excited in the hollow-cathode discharge tube in the spectral region 2140-2730 Å. Some $^{14}\text{N}^{18}\text{O}$ heads occur as impurities in the $^{14}\text{N}^{16}\text{O}$ spectra. These spectra are photographed on the 2 m Bausch and Lomb spectrograph in the first order of a 600 grooves/mm grating.

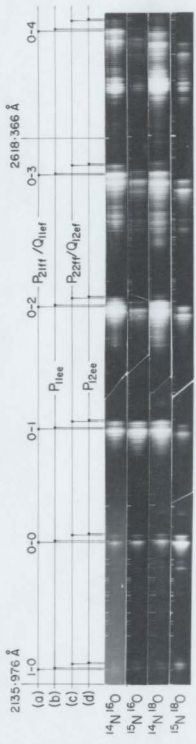


Table 4.1: Band heads of the γ ($A^2\Sigma^+ - X^2\Pi$) system of the $^{14}\text{N}^{16}\text{O}$ molecule

Band head ^{a,b} (cm^{-1})	Relative intensity	Assignment $v' - v''$
46394.1	vw	1-0
46420.3		
46520.3		
46541.0		
44051.7	w	0-0
44076.4		
44174.2		
44194.4		
42177.8	s	0-1
42201.3		
42300.8		
42320.9		
40332.5	s	0-2
40354.3		
40454.9		
40473.1		
38513.6	vs	0-3
38534.1		
38636.2		
38653.1		
36723.8	s	0-4
36742.8		
36845.4		
36864.1		

^aThe four heads for each band are formed by the P_{12e} , P_{22f}/Q_{12e} , P_{11e} and P_{21f}/Q_{11e} branches in the order of increasing wave number.

^bFrom the medium dispersion spectra.

^cThe abbreviations for the relative intensities vs, s, m, w and vw represent very strong, strong, medium, weak and very weak, respectively.

Table 4.2: Band heads of the γ ($A^2\Sigma^+ - X^2\Pi$) system of the $^{15}\text{N } ^{16}\text{O}$ molecule

Band head ^{a,b} (cm^{-1})	Relative intensity	Assignment $v' - v''$
46347.6 46370.9 46470.7 46488.4	w	1-0
44047.5 44071.2 44172.1 44193.0	m	0-0
42207.8 42230.3 42330.4 42350.9	s	0-1
40393.5 40414.8 40517.7 40534.6	s	0-2
38606.2 38625.9 38726.9 38745.2	vs	0-3
36846.0 36864.7 36967.9 36984.2	s	0-4

^aThe four heads identified for each band are formed by the P_{12e} , P_{22f}/Q_{12e} , P_{11e} and P_{21f}/Q_{11e} branches in the order of increasing wave number.

^bFrom the medium dispersion spectra.

^cThe abbreviations for the relative intensities vs, s, m, w and vw represent very strong, strong, medium, weak and very weak, respectively.

Table 4.3: Band heads of the γ ($A^2\Sigma^- - X^2\Pi$) system of the $^{14}\text{N}^{18}\text{O}$ molecule

Band head ^{a,b} (cm^{-1})	Relative intensity	Assignment $v' - v''$
46329.3	vw	1-0
46354.9		
46453.9		
46470.6		
44049.6	m	0-0
44072.8		
44171.1		
44187.9		
42221.4	s	0-1
42243.8		
42341.6		
42360.4		
40422.3	s	0-2
40442.9		
40544.3		
40560.8		
38649.5	vs	0-3
38669.3		
38770.9		
38787.2		
36903.3	s	0-4
36920.4		
37024.9		
37039.3		

^aThe four heads identified for each band are formed by the $P_{12e}, P_{22f}/Q_{12e}, P_{11e}$ and P_{21f}/Q_{11e} branches in the order of increasing wave number.

^bFrom the medium dispersion spectra.

^cThe abbreviations for the relative intensities vs, s, m, w and vw represent very strong, strong, medium, weak and very weak, respectively.

Table 4.4: Band heads of the γ ($A^2\Sigma^+ - X^2\Pi$) system of the $^{15}\text{N}^{18}\text{O}$ molecule

Band head ^{a,b} (cm^{-1})	Relative intensity	Assignment $v' - v''$
46280.6	w	1-0
46305.5		
46404.3		
46426.6		
44044.8	m	0-0
44068.4		
44171.2		
44189.5		
42252.31	s	0-1
42273.92		
42375.99		
42394.27		
40486.36	s	0-2
40506.52		
40609.25		
40626.65		
38746.01	vs	0-3
38764.86		
38868.29		
38884.54		
37030.3	s	0-4
37048.0		
37152.0		
37167.2		

^aThe four heads identified for each band are formed by the P_{12ef} , P_{21ff}/Q_{12ef} , P_{11ef} and P_{21ff}/Q_{11ef} branches in the order of increasing wave number.

^bThe 1-0, 0-0 and 0-4 band heads are measured under the medium dispersion and the 0-1, 0-2 and 0-3 band heads are measured under the high dispersion.

^cThe abbreviations for the relative intensities vs, s, m, w and vw represent very strong, strong, medium, weak and very weak, respectively.

Table 4.5: Deslandres table of band heads^a (in cm^{-1}) of the γ ($A^2\Sigma^+ - X^2\Pi$) system of the $^{14}N^{16}O$ molecule

v' \ v''	0	1	2	3	4
	$\Delta G''(1/2)$	$\Delta G''(3/2)$	$\Delta G''(5/2)$	$\Delta G''(7/2)$	
0	44051.7	42177.8	40332.5	38513.6	36723.8
	1873.9	1845.3	1819.9	1789.8	
	44076.4	42201.3	40354.3	38534.1	36742.8
	1875.1	1847.0	1820.2	1791.3	
	44174.2	42300.8	40454.9	38636.2	36845.4
	1873.4	1845.9	1818.7	1790.8	
	44194.4	42320.9	40473.1	38653.1	36864.1
	1873.5	1847.8	1820.0	1789.0	
	$\Delta G'(1/2)$				
	2342.4				
	2343.9				
	2346.1				
	2346.6				
1	46394.1				
	46420.3				
	46520.3				
	46541.0				

^aThe four heads for each band are formed by the P_{12ef} , P_{22ff}/Q_{12ef} , P_{11ef} and P_{21ff}/Q_{11ef} branches in the order of increasing wave number.

Table 4.7: Deslandres table of band heads^a (in cm^{-1}) of the γ ($A^2\Sigma^+ - X^2\Pi$) system of the $^{14}\text{N}^{18}\text{O}$ molecule

v', v''	0	1		2		3		4	
0		$\Delta G''(1/2)$		$\Delta G''(3/2)$		$\Delta G''(5/2)$		$\Delta G''(7/2)$	
	44049.6	1828.2	42221.4	1799.1	40422.3	1772.8	38649.5	1746.2	36903.3
	44072.8	1829.0	42243.8	1800.9	40442.9	1773.6	38669.3	1748.9	36920.4
	44171.1	1826.5	42344.6	1800.3	40544.3	1773.4	38770.9	1746.0	37024.9
	44187.9	1827.5	42360.4	1799.6	40560.8	1773.6	38787.2	1747.9	37039.3
	$\Delta G'(1/2)$								
	2279.7								
	2282.1								
	2282.8								
	2282.7								
1	46329.3								
	46354.9								
	46453.9								
	46470.6								

^aThe four heads for each band are formed by the P_{12ee} , P_{22ff}/Q_{12ef} , P_{11ee} and P_{31ff}/Q_{11ef} branches in the order of increasing wave number.

Table 4.8: Deslandres table of band heads^a (in cm^{-1}) of the γ ($\Lambda^2\Sigma^+-X^2\Pi$) system of the $^{15}\text{N}^{18}\text{O}$ molecule

v', v''	0	1	2	3	4
0	$\Delta G'(1/2)$	$\Delta G''(3/2)$	$\Delta G''(5/2)$	$\Delta G''(7/2)$	
	-44014.8	1792.5	42252.31	1765.95	40486.36
	-44068.4	1794.5	42273.92	1767.40	40506.52
	-44171.2	1795.2	42375.99	1766.74	40609.25
	-44189.5	1795.2	42394.27	1767.62	40626.65
	$\Delta G'(1/2)$				
	2235.8				
	2237.1				
	2235.1				
	2237.1				
1	-46280.6				
	-46305.5				
	-46404.3				
	-46426.6				

^aThe four heads for each band are formed by the P_{12ee} , P_{21ff}/Q_{12ef} , P_{11ee} and P_{21ff}/Q_{11ef} branches in the order of increasing wave number.

Table 4.9: Vibrational constants^a (in cm^{-1}) of the $X^2\Pi$ and $A^2\Sigma^+$ states of $^{14}\text{N}^{16}\text{O}$, $^{15}\text{N}^{16}\text{O}$, $^{14}\text{N}^{18}\text{O}$ and $^{15}\text{N}^{18}\text{O}$ obtained from the band-head data

State	Constant	$^{15}\text{N}^{16}\text{O}$		$^{14}\text{N}^{18}\text{O}$		$^{15}\text{N}^{18}\text{O}$	
		Observed value	Calculated value	Observed value	Calculated value	Observed value	Calculated value
$A^2\Sigma^+$	$\Delta G'(1/2)$	2345.3		2297.6		2282.4	2237.1
$X^2\Pi_{3/2}$	ω_e	1902.9 ₅ (0.6)	1868.9 ₂	1868.0 ₅ (0.8)	1855.0 ₀ (1.3)	1852.8 ₃	^b
	$\omega_e x_e$	13.9 ₁ (0.3)	13.4 ₁	13.2 ₀ (0.4)	13.3 ₈ (0.6)	13.1 ₉	^b
$X^2\Pi_{1/2}$	ω_e	1902.9 ₀ (1.9)	1868.8 ₈	1869.7 ₁ (0.9)	1853.3 ₅ (0.8)	1852.7 ₈	^b
	$\omega_e x_e$	14.0 ₇ (0.8)	13.5 ₇	13.5 ₁ (0.4)	13.2 ₄ (0.4)	13.3 ₄	^b

^aNumber in the parenthesis is the uncertainty and corresponds to one standard deviation.

^bThe vibrational constant is obtained from the band-origin data derived from the rotational analysis.

4.2 Rotational Analysis of the 0-1, 0-2 and 0-3 bands of $^{15}\text{N}^{18}\text{O}$

The γ system of $^{15}\text{N}^{18}\text{O}$ was photographed under high resolution in the fifth order of a 1200 grooves/mm grating on the 3.1 m Jarrell-Ash spectrograph. Of all the bands attempted, the 0-1, 0-2, 0-3 and 0-4 bands were recorded with measurable intensity. The rotational analysis of the 0-1, 0-2 and 0-3 bands is carried out, but that of the 0-4 band is not done as it is overlapped with an impurity spectrum. Iron and neon lines from Fe-Ne hollow-cathode lamp, photographed in the fourth order of the grating, were used as wavelength standards.

The γ system of nitric oxide arises from the transition $A^2\Sigma^+ - X^2\Pi_r$. The upper $A^2\Sigma^+$ state belongs to Hund's case (b) and the lower $X^2\Pi_r$ state normally belongs to Hund's case (a) (see below). The rotational structure of a band arising from a $A^2\Sigma^+ - X^2\Pi_r$ transition gives rise to 12 branches which are designated as P_{12ee} , P_{22ff} , Q_{12ef} , Q_{22fe} , R_{12ee} and R_{22ff} , from ${}^2\Sigma^+ - {}^2\Pi_{3/2} (F_2)$, and P_{11er} , P_{21ff} , Q_{11ef} , Q_{21fr} , R_{11ee} and R_{21ff} , from ${}^2\Sigma^+ - {}^2\Pi_{1/2} (F_1)$. These twelve branches of a band, degraded to shorter wavelengths, are schematically shown in Figure 3.1. The labelling of the parity of the levels in the *ef* notation is given according to Brown *et al* (1975). As the bands of this system are degraded to shorter wavelengths, the P_{12ee} and P_{22ff}/Q_{12ef} branches from ${}^2\Sigma^+ - {}^2\Pi_{3/2}$ and P_{11er} and Q_{11ef}/P_{21ff} branches from ${}^2\Sigma^+ - {}^2\Pi_{1/2}$ form four distinct heads in the rotational structure of a band. The characteristic band origin $T'_v - T''_v$ is estimated from the analysis (see below). The band origins of the ${}^2\Sigma^+ - {}^2\Pi_{3/2}$ and ${}^2\Sigma^+ - {}^2\Pi_{1/2}$ subbands of a band are obtained from the relation $(T'_v - T''_v) \pm (1/2)(A_v - 2B_v)$, where A_v is the spin-orbit coupling constant of the ${}^2\Pi$ state and B_v is its rotational constant. The effective Hamiltonian for the ${}^2\Sigma^+$ and ${}^2\Pi$

states of diatomic molecules, discussed in detail by Brown *et al* (1979) (see Section 3 in Chapter 3) was used in the analysis of the 0-1, 0-2 and 0-3 bands of the γ system of $^{15}\text{N}^{18}\text{O}$. Amiot *et al* (1981) gave a complete list of the matrix elements of this Hamiltonian and the matrix elements used in the present analysis are listed in Table 3.1.

The rotational structure of the 0-2 band of the γ system of $^{15}\text{N}^{18}\text{O}$ photographed under high resolution on the 3.4 m Jarrell-Ash spectrograph is shown in Figure 4.2. In this figure the four heads and the twelve branches expected in a $^2\Sigma^+ - ^2\Pi$ transition are identified. As the spin splitting of the rotational levels of the $A^2\Sigma^+$ state is very small, the γ_v values could not be estimated.

The rotational quantum numbers of the vacuum wavenumbers of the spectral lines of the 0-1, 0-2 and 0-3 bands of the γ system of $^{15}\text{N}^{18}\text{O}$ are listed in Table 4.10. The vacuum wavenumbers of the spectral lines of all the twelve branches of a given band were simultaneously used as input to the nonlinear least-squares program and the molecular constants and their standard deviations were obtained. The values of $(\nu_{\text{obs}} - \nu_{\text{cal}})$ obtained from the least-squares fit of the wavenumbers of the bands are given in parentheses in Table 4.10. In general, the standard deviation of the least-squares fit is found to be about 0.05 cm^{-1} . As seen from the Fortrat diagram plotted in Figure 4.3 for the 0-2 band, the wavenumbers of the corresponding pairs of branches, P_{11ee} and P_{22ff} , Q_{11ef} and Q_{22fe} , and R_{11ee} and R_{22ff} , become closer and closer together with increasing J . This indicates clearly the transition from case (a) to case (b)(see Herzberg, 1950, p. 262).

Figure 4.2 Rotational structure of the 0-2 band of the ν ($A^{2\Sigma^+ - X^2\Pi$) system of $^{15}\text{N}^{18}\text{O}$, photographed on the 3.4 m Jarrell-Ash spectrograph in the fifth order of a 1200 grooves/mm grating.

Table 4.10: Vacuum wavenumbers^a (in cm^{-1}) of the rotational lines of the ν ($A^2\Sigma^+-X^2\Pi$) system of $^{15}N^{18}O$

0-1 band						
J	$P_{12ee}(J)$	$P_{22ff}(J)$	$Q_{12ef}(J)$	$Q_{22fe}(J)$	$R_{12ee}(J)$	$R_{22ff}(J)$
0.5						
1.5	42270.70(- 8)	42274.42(1)	42274.42(1)	42281.75(9)	42281.75(9)	42292.67(13)
2.5	266.74(10)	273.92(2)	273.92(2)	284.88(10)	284.88(10)	
3.5	263.84 ^b	273.92(1)	273.92(1)	288.53(11)	288.53(11)	
4.5	260.72 ^b	274.42(- 2)	274.42(- 2)	292.67(10)	292.67(10)	314.43(10)
5.5	257.42(6)	275.50(1)	275.50(1)	297.29(3)	297.29(3)	
6.5	255.49 ^b	276.95(-12)	276.95(-12)	302.52(6)	302.52(6)	331.50(5)
7.5	253.90(11)	279.11(- 6)	279.11(- 6)	308.10(- 7)	308.10(- 7)	
8.5	252.81(3)	281.75(- 4)	281.75(- 4)	314.43(1)	314.43(1)	350.66(- 1)
9.5	252.31(0)	284.88(- 6)	284.88(- 6)	321.19(0)	321.19(0)	361.06(0)
10.5	252.31(- 5)	288.53(- 8)	288.53(- 8)	328.48(- 1)	328.48(- 1)	371.99(1)
11.5	252.81(-12)	292.67(-14)	292.67(-14)	336.31(1)	336.31(1)	383.39(- 2)
12.5	253.90(-15)	297.52(- 1)	297.52(- 1)	344.58(- 6)	344.58(- 6)	395.48(11)
13.5	255.49 ^b	302.75(- 4)	302.75(- 4)	353.48(- 3)	353.48(- 3)	407.86(1)
14.5	257.87(4)	308.57(1)	308.57(1)	362.85(- 6)	362.85(- 6)	420.86(0)
15.5	260.72 ^b	314.80(- 7)	314.80(- 7)	372.80(- 3)	372.80(- 3)	434.34(- 5)
16.5	263.84(9)	321.72(1)	321.72(1)	383.17(-11)	383.17(-11)	448.45(0)
17.5	267.63(12)	329.08(0)	329.08(0)	394.27(0)	394.27(0)	463.00(- 5)
18.5	271.91(10)	336.97(- 1)	336.97(- 1)	405.76(- 2)	405.76(- 2)	478.16(0)
19.5		345.40(- 2)	345.40(- 2)	417.78(- 4)	417.78(- 4)	493.58 ^b
20.5		354.39(0)	354.39(0)	430.40(1)	430.40(1)	509.93(- 6)
21.5		363.90(1)	363.90(1)	443.55(5)	443.55(5)	
22.5		373.88(- 5)	373.88(- 5)	457.15(1)	457.15(1)	

Table 4.10 (Continued)

0-1 band (continued)						
J	$P_{12e}(J)$	$P_{22f}(J)$	$Q_{12e}(J)$	$Q_{22f}(J)$	$R_{12e}(J)$	$R_{22f}(J)$
23.5		384.46(- 5)	384.46(- 5)	-171.22(-10)	471.22(-10)	
24.5		395.48(-14)	395.48(-14)	-186.03(1)	486.03(1)	
25.5		407.27(0)	407.27(0)	501.31(- 4)	501.31(- 4)	
26.5		419.48(1)	419.48(1)	517.10(5)	517.10(5)	
27.5		432.22(2)	432.22(2)	533.34(- 3)	533.34(- 3)	
28.5		445.50(3)	445.50(3)	550.23(0)	550.23(0)	
29.5		459.29(0)	459.29(0)	567.55(- 7)	567.55(- 7)	
30.5		473.57(- 8)	473.57(- 8)	585.55(- 1)	585.55(- 1)	
31.5		488.49(- 5)	488.49(- 5)	604.10(6)	604.10(6)	
32.5		504.04(5)	504.04(5)	623.05(- 1)	623.05(- 1)	
33.5		519.99(1)	519.99(1)	642.64(2)	642.64(2)	
34.5		536.55(3)	536.55(3)	662.73(0)	662.73(0)	
35.5		553.49(-12)	553.49(-12)	683.39(2)	683.39(2)	
36.5		571.18(- 5)	571.18(- 5)	704.61(5)	704.61(5)	
37.5		589.34(- 8)	589.34(- 8)	726.34(5)	726.34(5)	
38.5		608.20(5)	608.20(5)	748.58(2)	748.58(2)	
39.5		627.18 ^b	627.18 ^b	771.35(- 4)	771.35(- 4)	
-10.5		647.38(12)	647.38(12)	794.71(- 4)	794.71(- 4)	
-11.5		667.53(-10)	667.53(-10)	818.67(1)	818.67(1)	
-12.5		688.55(0)	688.55(0)			

Table 4.10 (Continued)

J	0-1 band (continued)					
	$P_{11ee}(J)$	$P_{21ff}(J)$	$Q_{11ef}(J)$	$Q_{21fe}(J)$	$R_{11ee}(J)$	$R_{21ff}(J)$
0.5						
1.5						
2.5				-42404.95(3)	-42404.95(3)	-42419.48(9)
3.5	-42383.39(- 5)	-42394.27(- 1)	-42394.27(- 1)	-408.75(- 8)	-408.75(- 8)	
4.5	380.41 ^b	395.12(- 4)	395.12(- 5)	-413.19(-15)	-413.19(-15)	-434.34 ^b
5.5	378.40 ^b	396.64(0)	396.64(0)	-418.39(- 6)	-418.39(- 6)	-443.56 ^b
6.5	376.98(- 5)	398.71(0)	398.71(0)	-424.07(- 9)	-424.07(- 9)	-452.99(-11)
7.5	375.99(- 9)	-401.41(2)	-401.41(2)	-430.40(- 7)	-430.40(- 7)	-463.00(- 2)
8.5	375.99 ^b	-404.63(- 2)	-404.63(- 2)	-437.40(3)	-437.40(3)	-473.57(3)
9.5	375.99(0)	-408.55(2)	-408.55(2)	-444.92(5)	-444.92(5)	
10.5	376.98(13)	-412.86(-13)	-412.86(-13)	-452.99(3)	-452.99(3)	
11.5	378.40(11)	-418.05(0)	-418.05(0)	-461.57(- 9)	-461.57(- 9)	508.64(- 1)
12.5	380.41(8)	-423.70(0)	-423.70(0)	-470.97(4)	-470.97(4)	521.44(-10)
13.5	383.17 ^b	-429.98(3)	-429.98(3)	-480.82(1)	-480.82(1)	
14.5	386.17(- 4)	-436.77(- 2)	-436.77(- 2)	-491.26(- 2)	-491.26(- 2)	
15.5	389.92(-10)	-444.25(2)	-444.25(2)	-502.38(5)	-502.38(5)	
16.5	394.27 ^b	-452.27(2)	-452.27(2)	-513.95(- 2)	-513.95(- 2)	
17.5	399.45(- 1)	-460.81(- 5)	-460.81(- 5)	-526.18(- 3)	-526.18(- 3)	
18.5	404.95(-12)	-470.06(- 1)	-470.06(- 1)	-539.00(- 3)	-539.00(- 3)	
19.5	411.38(12)	-479.89(2)	-479.89(2)	-552.47(3)	-552.47(3)	
20.5	418.05(1)	-490.27(2)	-490.27(2)	-566.43(- 1)	-566.43(- 1)	
21.5	425.49(8)	-501.17(- 5)	-501.17(- 5)	-580.93(- 8)	-580.93(- 8)	
22.5	433.42(5)	-512.75(- 1)	-512.75(- 1)	-596.18(1)	-596.18(1)	
23.5	441.87(- 5)	-524.89(- 2)	-524.89(- 2)	-611.91(0)	-611.91(0)	
24.5	451.16(10)	-537.64(2)	-537.64(2)	-628.27(3)	-628.27(3)	
25.5	460.81(3)	-550.89(- 4)	-550.89(- 4)	-645.16(1)	-645.16(1)	

Table 4.10 (Continued)

J	0-1 band (continued)					
	$P_{11,e}(J)$	$P_{21,f}(J)$	$Q_{11,e}(J)$	$Q_{21,f}(J)$	$R_{11,e}(J)$	$R_{21,f}(J)$
26.5	170.97(-11)	564.84(2)	564.84(2)	562.73(9)	662.73(9)	
27.5	181.96(- 1)	579.27(- 2)	579.27(- 2)	680.70(0)	680.70(0)	
28.5	493.58(13)	594.37(2)	594.37(2)	699.31(- 4)	699.31(- 4)	
29.5	505.50(0)	610.03(6)	610.03(6)	718.57(1)	718.57(1)	
30.5	518.18(- 4)	626.18(- 1)	626.18(- 1)	738.38(2)	738.38(2)	
31.5	531.24(-11)	643.03(5)	643.03(5)	758.68(- 5)	758.68(- 5)	
32.5	545.25(9)	660.40(6)	660.40(6)	779.58(-10)	779.58(-10)	
33.5	559.65(11)	678.32(3)	678.32(3)	801.24(5)	801.24(5)	
34.5	574.61(-14)	696.84(3)	696.84(3)	823.24(- 4)	823.24(- 4)	
35.5	590.05(1)	715.91(1)	715.91(1)	845.91(- 4)	845.91(- 4)	
36.5	606.30(14)	735.65(8)	735.65(8)	869.20(2)	869.20(2)	
37.5	623.05 ^a	755.79(- 3)	755.79(- 3)	892.87(-11)	892.87(-11)	
38.5	640.21(8)	776.62(- 2)	776.62(- 2)			
39.5		797.97(- 6)	797.97(- 6)			
40.5		819.88(-11)	819.88(-11)			
41.5		842.55(2)	842.55(2)			
42.5		865.56(- 8)	865.56(- 8)			
43.5		889.32(1)	889.32(1)			

Table 4.10 (Continued)

0-2 band						
J	$P_{12e_f}(J)$	$P_{22f_f}(J)$	$Q_{12e_f}(J)$	$Q_{22f_f}(J)$	$R_{12e_f}(J)$	$R_{22f_f}(J)$
0.5						
1.5		10507.22 ^b	-10507.22 ^b			
2.5		506.52(8)	506.52(8)	-10517.45(13)	10517.45(13)	
3.5	40495.71(3)	506.52(- 4)	506.52(- 1)	521.19(12)	521.19(12)	
4.5	492.83(10)	507.22(- 1)	507.22(- 1)	525.34(- 3)	525.34(- 3)	10547.36 ^b
5.5	490.36(3)	508.17(1)	508.17(1)	530.21(2)	530.21(2)	555.19 ^b
6.5	488.68 ^b	510.21(- 4)	510.21(- 4)	535.63(0)	535.63(0)	
7.5	487.30(10)	512.59(1)	512.59(1)	541.52(- 6)	541.52(- 6)	574.27(6)
8.5	486.55(8)	515.13(- 4)	515.13(- 4)	548.08(- 2)	548.08(- 2)	584.17 ^b
9.5	486.36(6)	518.92(0)	518.92(0)	555.19(2)	555.19(2)	595.11(8)
10.5	486.65(- 3)	522.91(- 1)	522.91(- 1)	562.76(- 3)	562.76(- 3)	606.34(7)
11.5	487.67(5)	527.19(1)	527.19(1)	570.90(- 2)	570.90(- 2)	618.18(10)
12.5	489.13(1)	532.62(1)	532.62(1)	579.70(- 2)	579.70(- 2)	630.57(14)
13.5	491.29(10)	538.26(- 3)	538.26(- 3)	589.00(- 1)	589.00(- 1)	643.45(11)
14.5	493.94(12)	544.50(- 3)	544.50(- 3)	598.90(3)	598.90(3)	656.58 ^b
15.5	497.08(8)	511.29(- 4)	511.29(- 4)	609.25(- 3)	609.25(- 3)	670.86(3)
16.5	500.77(2)	558.68(0)	558.68(0)	620.25(- 0)	620.25(- 0)	685.51(10)
17.5	505.19(13)	566.61(1)	566.61(1)	631.72(- 7)	631.72(- 7)	700.65(10)
18.5	510.21 ^b	575.10(1)	575.10(1)	643.91(2)	643.91(2)	716.12(12)
19.5	515.13(- 4)	584.17(3)	584.17(3)	655.58(3)	655.58(3)	732.56(6)
20.5		593.77(2)	593.77(2)	669.77(1)	669.77(1)	749.37(5)
21.5		603.96(2)	603.96(2)	683.56(1)	683.56(1)	766.71(1)
22.5		614.70(1)	614.70(1)	697.97(7)	697.97(7)	784.71(8)
23.5		626.11(11)	626.11(11)	712.80(- 1)	712.80(- 1)	803.26(11)
24.5		637.85(- 3)	637.85(- 3)	728.30(1)	728.30(1)	822.30(10)
25.5		650.33(- 1)	650.33(- 1)	744.33(- 2)	744.33(- 2)	841.90(7)

Table 4.10 (Continued)

J	0-2 band (continued)					
	$P_{12e}(J)$	$P_{22f}(J)$	$Q_{12e}(J)$	$Q_{22e}(J)$	$R_{12e}(J)$	$R_{22f}(J)$
26.5	663.33(- 3)	663.33(- 3)	760.99(- 4)	760.99(- 4)	862.09(- 6)	
27.5	676.94(- 1)	676.94(- 1)	778.12(- 2)	778.12(- 2)	882.86(- 8)	
28.5	691.09(- 3)	691.09(- 3)	795.90(- 1)	795.90(- 1)	904.19(- 9)	
29.5	705.82(- 1)	705.82(- 4)	814.19(- 2)	814.19(- 2)	926.03(- 4)	
30.5	721.18(- 1)	721.18(- 1)	833.06(- 5)	833.06(- 5)	948.47(- 3)	
31.5	737.09(- 3)	737.09(- 3)	852.69(- 12)	852.69(- 12)	971.52(- 6)	
32.5	753.53(- 1)	753.53(- 1)	872.61(- 1)	872.61(- 1)	995.03(- 2)	
33.5	770.45(-10)	770.45(-10)	893.22(- 1)	893.22(- 1)	1019.26(- 5)	
34.5	788.06(-11)	788.06(-11)	914.39(- 0)	914.39(- 0)	044.00(- 6)	
35.5	806.38(- 3)	806.38(- 3)	936.13(- 1)	936.13(- 1)	069.28(- 6)	
36.5	825.20(- 8)	825.20(- 8)	958.45(- 2)	958.45(- 2)	095.11(- 3)	
37.5	844.46(- 0)	844.46(- 0)	981.36(- 1)	981.36(- 1)	121.99 ^b	
38.5	864.39(- 0)	864.39(- 0)	-1004.81(- 3)	-1004.81(- 3)	148.61(- 10)	
39.5	884.85(- 4)	884.85(- 4)	028.87(- 2)	028.87(- 2)	176.25 ^b	
40.5	905.90(- 8)	905.90(- 8)	053.46(- 5)	053.46(- 5)	204.13(-10)	
41.5			078.64(- 7)	078.64(- 7)		
42.5			104.49(- 0)	104.49(- 0)		
43.5			130.79(- 5)	130.79(- 5)		

Table 4.10 (Continued)

0-2 band (continued)						
J	$P_{11ee}(J)$	$P_{21ff}(J)$	$Q_{11ee}(J)$	$Q_{21ff}(J)$	$R_{11ee}(J)$	$R_{21ff}(J)$
0.5						10638.23 ^k
1.5		40626.65(0)	40626.65(0)	40633.91(- 2)	40633.91(2)	643.91 ^k
2.5	40619.08(-10)	626.65 ^b	626.65 ^b	637.34(2)	637.34(2)	651.28 ^k
3.5	615.17 ^b	626.65(-14)	626.65(-14)	641.42(8)	641.42(8)	659.49(7)
4.5	613.41(5)	627.78(- 2)	627.78(- 2)	646.00(1)	646.00(1)	667.75(7)
5.5	611.07 ^b	629.44(- 1)	629.44(- 1)	651.28(1)	651.28(1)	676.94 ^k
6.5	609.90 ^b	631.72(1)	631.72(1)	657.04(-14)	657.04(-11)	686.28 ^k
7.5	609.25(- 8)	634.61(0)	634.61(0)	663.68(- 3)	663.68(- 3)	696.15(-10)
8.5	609.25(1)	638.24(10)	638.24(10)	670.86(- 1)	670.86(- 1)	707.72 ^k
9.5	609.90(12)	642.26(- 3)	642.26(- 3)	678.67(1)	678.67(1)	718.20 ^k
10.5	611.07(11)	647.96(- 1)	647.96(- 1)	687.08(1)	687.08(1)	730.57(15)
11.5	612.74(- 1)	652.45(- 3)	652.45(- 3)	696.15(4)	696.15(4)	
12.5	615.17(- 1)	658.50(0)	658.50(0)	705.82(5)	705.82(5)	756.60 ^k
13.5	618.18(- 4)	665.10(- 6)	665.10(- 6)	716.12(8)	716.12(8)	770.45 ^k
14.5	621.88(- 1)	672.43(- 1)	672.43(- 1)	726.97(2)	726.97(2)	784.71(- 1)
15.5	626.11(- 8)	680.33(- 1)	680.33(- 1)	738.42(- 5)	738.42(- 5)	
16.5	631.15(- 4)	688.86(0)	688.86(0)	750.61(0)	750.61(0)	
17.5	636.66(1)	697.97(- 3)	697.97(- 3)	763.37(- 1)	763.37(- 1)	
18.5	642.83(2)	707.73(- 4)	707.73(- 4)	776.76(1)	776.76(1)	
19.5	649.55(- 5)	718.21(6)	718.21(6)	790.74(- 1)	790.74(- 1)	
20.5	657.04(- 4)	729.17(2)	729.17(2)	815.37(1)	815.37(1)	
21.5	665.10(7)	740.79(2)	740.79(2)	829.56(- 2)	829.56(- 2)	
22.5	673.66(- 1)	753.01(1)	753.01(1)	836.42(- 1)	836.42(- 1)	
23.5	682.96(3)	675.88(3)	675.88(3)	852.68 ^b	852.68 ^b	
24.5	692.76(- 4)	779.29(- 2)	779.29(- 2)	869.96(2)	869.96(2)	
25.5	703.30(1)	793.41(2)	793.41(2)	887.61(- 1)	887.61(- 1)	

Table 4.10 (Continued)

J	$P_{11\rightarrow}(J)$	$P_{21f}(J)$	0-2 band (continued)			
			$Q_{11e}(J)$	$Q_{21e}(J)$	$R_{11e}(J)$	$R_{21e}(J)$
26.5	714.11(1)	808.14(5)	808.14(5)	905.90(0)	905.90(0)	
27.5	726.17(1)	823.38(- 1)	823.38(- 1)	924.79(0)	924.79(0)	
28.5	738.42(- 5)	839.31(1)	839.31(1)	944.25(- 4)	944.25(- 1)	
29.5	751.38(- 3)	885.84(1)	885.84(1)	964.38(- 1)	964.38(- 1)	
30.5	765.01(1)	872.98(2)	872.98(2)	985.03(- 7)	985.03(- 7)	
31.5	779.29(14)	890.74(4)	890.74(4)	41006.39(- 3)	41006.39(- 3)	
32.5	793.99(0)	909.07(2)	909.07(2)	028.29(- 5)	028.29(- 5)	
33.5	809.41(8)	928.01(0)	928.01(0)	050.86(- 1)	050.86(- 1)	
34.5	825.20(- 14)	947.56(- 1)	947.56(- 1)	074.00(1)	074.00(1)	
35.5	841.90(- 5)	967.75(1)	967.75(1)	097.70(- 2)	097.70(- 2)	
36.5	859.19(1)	988.43(- 8)	988.43(- 8)	121.99(- 6)	121.99(- 6)	
37.5	877.03(2)	11009.87(- 1)	41009.87(- 1)	146.92(- 5)	146.92(- 5)	
38.5	895.48(3)	031.89(2)	031.89(2)	172.48(- 2)	172.48(- 2)	
39.5	914.39(- 10)	054.46(1)	054.46(1)	198.63(1)	198.63(1)	
40.5	934.14(- 1)	077.64(- 0)	077.64(- 0)	225.33(- 1)	225.33(- 1)	
41.5		101.44(2)	101.44(2)			
42.5		125.82(1)	125.82(1)			
43.5		150.80(0)	150.80(0)			
44.5		176.25(- 13)	176.25(- 13)			
45.5		202.58(1)	202.58(1)			

Table 4.10 (Continued)

0.3 band						
J	$P_{12e}(J)$	$P_{22e'}(J)$	$Q_{12e'}(J)$	$Q_{22e'}(J)$	$R_{12e'}(J)$	$R_{22e'}(J)$
0.5						
1.5	38761.46(- 4)			38772.49(11)	38772.49(11)	
2.5	758.09 ¹	38761.86(9)	38764.86(9)	775.61(- 3)	775.61(- 3)	
3.5	754.09(- 4)	764.99(0)	764.99(0)	779.46(- 4)	779.46(- 4)	
4.5	751.16(- 15)	765.90(9)	765.90(9)	783.81(- 10)	783.81(- 10)	
5.5	749.13(5)	767.21(0)	767.21(0)	789.00(3)	789.00(3)	
6.5	747.45(0)	769.18(- 2)	769.18(- 2)	794.58(1)	794.58(1)	
7.5	746.35(- 4)	771.74(- 3)	771.74(- 3)	800.76(- 1)	800.76(- 1)	
8.5	745.01 ¹	774.93(0)	774.93(0)	807.57(1)	807.57(1)	
9.5	746.01(- 4)	778.66(- 1)	778.66(- 1)	814.93(1)	814.93(1)	38854.87(9)
10.5	746.78(2)	783.00(0)	783.00(0)	822.89(2)	822.89(2)	866.44(8)
11.5	748.03(- 3)	787.91(- 1)	787.91(- 1)	831.38(- 3)	831.38(- 3)	878.13(- 9)
12.5	749.88(- 7)	793.43(1)	793.43(1)	840.51(- 3)	840.51(- 3)	891.24(2)
13.5	752.34(- 9)	799.52(- 1)	799.52(- 1)	850.25(- 1)	850.25(- 1)	904.30 ^h
14.5	756.12 ¹	806.22(0)	806.22(0)	860.59(2)	860.59(2)	919.01 ^h
15.5	759.26(8)	813.52(2)	813.52(2)	871.47(1)	871.47(1)	932.92(- 9)
16.5	763.45(1)	821.37(- 1)	821.37(- 1)	882.98(3)	882.98(3)	948.10(- 1)
17.5		829.86(2)	829.86(2)	895.03(- 1)	895.03(- 1)	963.72(- 7)
18.5		838.90(0)	838.90(0)	907.70(0)	907.70(0)	979.99(- 8)
19.5		848.55(- 1)	848.55(- 1)	920.98(1)	920.98(1)	996.81(- 13)
20.5		858.80(- 2)	858.80(- 2)	934.81(- 3)	934.81(- 3)	39014.40(0)
21.5		869.68(2)	869.68(2)	949.33(- 4)	949.33(- 4)	032.38(- 7)
22.5		881.11(- 1)	881.11(- 1)	964.32(- 2)	964.32(- 2)	051.12(2)
23.5		893.26(10)	893.26(10)	979.99(0)	979.99(0)	069.82 ^h
24.5		905.88(7)	905.88(7)	996.23(- 1)	996.23(- 1)	090.99(- 8)
25.5		919.01(- 4)	919.01(- 4)	39012.92(- 16)	39012.92(- 11)	110.54(- 6)

Table 4.10 (Continued)

0-3 band (continued)						
J	$P_{122r}(J)$	$P_{221f}(J)$	$Q_{12rf}(J)$	$Q_{22fe}(J)$	$R_{12ee}(J)$	$R_{22ff}(J)$
26.5		932.92(1)	932.92(1)	030.19(- 1)	030.19(2)	
27.5		947.37(1)	947.37(1)	048.55(- 2)	048.55(3)	
28.5		962.40(- 1)	962.40(- 1)	067.11(- 8)	067.11(- 5)	
29.5		978.00(- 8)	978.00(- 8)	086.39(- 8)	086.39(- 1)	
30.5		994.31(- 3)	994.31(- 3)	106.25(- 7)	106.25(1)	
31.5		39011.16(- 6)	39011.16(- 6)	126.67(- 10)	126.67(- 2)	
32.5		028.66(- 13)	028.66(- 4)	147.74(- 8)	147.74(1)	
33.5		046.67(- 11)	046.67(- 11)	169.38(- 11)	169.38(- 1)	
34.5		065.53(5)	065.53(5)	191.66(- 9)	191.66(1)	
35.5		084.66(- 12)	084.66(- 12)			

Table 4.10 (Continued)

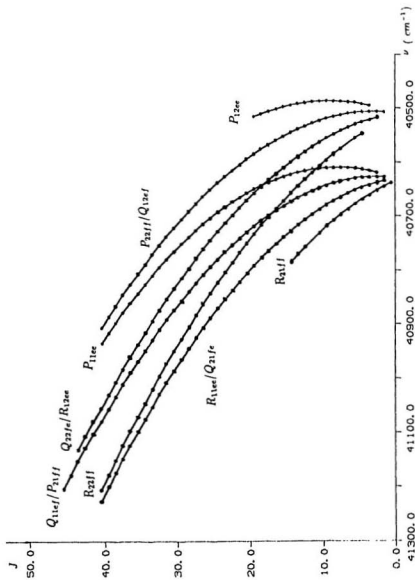
J	0-3 band (continued)					
	$P_{11\pi\pi}(J)$	$P_{21\pi\pi}(J)$	$Q_{11\pi\pi}(J)$	$Q_{21\pi\pi}(J)$	$R_{11\pi\pi}(J)$	$R_{21\pi\pi}(J)$
0.5						
1.5						
2.5		38884.54(- 5)	38884.54(- 5)			38909.76(- 12)
3.5		884.94(- 5)	884.94(- 5)	38899.46(- 7)	38899.46(- 7)	
4.5	38871.16 ⁺	886.10(- 3)	886.10(- 3)	904.31(- 0)	904.31(- 0)	925.98(- 3)
5.5	869.68 ^b	887.89(- 5)	887.89(- 5)	909.76(- 1)	909.76(- 1)	934.81 ⁺
6.5	868.74(- 2)	890.37(- 3)	890.37(- 3)	915.85(- 1)	915.85(- 1)	
7.5	868.29(- 7)	893.48(- 4)	893.48(- 4)	922.59(- 1)	922.59(- 1)	
8.5	868.29(- 9)	897.29(- 1)	897.29(- 1)	930.02(- 0)	930.02(- 0)	966.18(- 1)
9.5	869.22(- 1)	901.71(- 2)	901.71(- 2)	938.05(- 3)	938.05(- 3)	978.00(- 15)
10.5	870.70(- 2)	906.82(- 0)	906.82(- 0)	946.73(- 8)	946.73(- 8)	
11.5	872.82(- 0)	912.57(- 0)	912.57(- 0)	956.17(- 1)	956.17(- 1)	39003.16(- 0)
12.5	875.64(- 3)	919.01(- 4)	919.01(- 4)	966.18(- 3)	966.18(- 3)	
13.5	879.11(- 5)	925.98(- 5)	925.98(- 5)	976.86(- 3)	976.86(- 3)	031.00(- 9)
14.5	882.98 ^b	933.71(- 3)	933.71(- 3)	988.23(- 1)	988.23(- 1)	046.03 ⁺
15.5	887.89(- 3)	942.09(- 1)	942.09(- 1)	39000.21(- 1)	39000.21(- 1)	061.47(- 15)
16.5	893.26(- 6)	951.12(- 1)	951.12(- 1)	012.92(- 3)	012.92(- 3)	
17.5	899.46(- 8)	960.79(- 1)	960.79(- 1)	026.09(- 3)	026.09(- 3)	
18.5	906.13(- 4)	971.11(- 1)	971.11(- 1)	040.07(- 2)	040.07(- 2)	
19.5	913.53(- 6)	982.06(- 1)	982.06(- 1)	054.62(- 1)	054.62(- 1)	
20.5	921.55(- 7)	993.68(- 0)	993.68(- 0)	069.82(- 4)	069.82(- 4)	
21.5	930.02(- 12)	39005.94(- 0)	39005.94(- 0)	085.71(- 2)	085.71(- 2)	
22.5	939.52(- 7)	018.81(- 4)	018.81(- 4)	102.23(- 1)	102.23(- 1)	
23.5	949.33(- 9)	032.38(- 2)	032.38(- 2)	119.37(- 3)	119.37(- 3)	
24.5	960.13(- 11)	046.67(- 6)	046.67(- 6)	137.21(- 1)	137.21(- 1)	
25.5	971.11 ⁺	061.47(- 2)	061.47(- 2)	155.66(- 1)	155.66(- 1)	

Table 4.10 (Continued)

0-3 band (continued)						
<i>J</i>	<i>P</i> _{11<i>ee</i>} (<i>J</i>)	<i>P</i> _{21<i>ff</i>} (<i>J</i>)	<i>Q</i> _{11<i>ef</i>} (<i>J</i>)	<i>Q</i> _{21<i>fe</i>} (<i>J</i>)	<i>R</i> _{11<i>ee</i>} (<i>J</i>)	<i>R</i> _{21<i>ff</i>} (<i>J</i>)
26.5	983.27(9)	076.96(3)	076.96(3)	174.75(3)	174.75(3)	
27.5		093.07(0)	093.07(0)	194.50(5)	194.50(5)	
28.5		109.85(0)	109.85(0)	214.83(2)	214.83(2)	
29.5		127.26(0)	127.26(0)	235.81(- 1)	235.81(- 1)	
30.5		145.33(1)	145.33(1)	257.53(7)	257.53(7)	
31.5		164.04(3)	164.04(3)	279.78(5)	279.78(5)	
32.5		183.40(5)	183.40(5)	302.70(6)	302.70(6)	
33.5		203.34(1)	203.34(1)			
34.5		223.96(2)	223.96(2)			
35.5		245.18(- 2)	245.18(- 2)			
36.5		267.08(0)	267.08(0)			
37.5		289.54(- 7)	289.54(- 7)			

^aNumber in the parenthesis is the uncertainty in the last digit and corresponds to the difference between observed and calculated wavenumbers.

^bNot used in the analysis.

Figure 4.3 Fortrat diagram of the 0-2 band of the γ system of $^{15}\text{N}^{18}\text{O}$.

From the analysis of the individual bands, eight molecular parameters, B_v and D_v for the $A^2\Sigma^+$ state and B_v , D_v , A_v , A_{Dv} , p_v and q_v for the $X^2\Pi$, state and the band origins were estimated. The molecular constants thus obtained and their standard deviations for the 0-1, 0-2 and 0-3 bands of the A-X system of $^{15}\text{N}^{18}\text{O}$ are listed in Table 4.11, and the band origins are given in Table 4.12. The molecular constants, their standard deviations and the corresponding variance-covariance matrices were used as input parameters for the correlated least-squares fit in which the output data from the analysis of all three analyzed bands were merged together to reduce all the redundant values to a single value using a MERGE program.

The values of the molecular constants and the band origins obtained from the MERGE program are listed in Tables 4.13 and 4.14, respectively. The B_e values for the $X^2\Pi$ state were fitted to the relation (see Equation 3.14)

$$B_v = B_e - \alpha_e(v + 1/2), \quad (4.5)$$

and the equilibrium rotational constants B_e and α_e thus obtained are given in Table 4.15. From the band origins, the values of ω_e and $\omega_e x_e$ for the $X^2\Pi$ state were calculated (see Equation 3.6) and are also given in Table 4.15. As the values of D_e for $v = 1, 2$ and 3 vary irregularly, the value of D_e is calculated from the Kratzer's relation

$$D_e = 4B_e^3/\omega_e^2, \quad (4.6)$$

and is listed in Table 4.15. The equilibrium moment of inertia I_e and the intermolecular separation r_e obtained from the value of B_e are also listed in the same table. The term value of the A, $v = 0$ level and those of the $X^2\Pi$, $v=1, 2$, and 3 levels (note $^2\Pi$ $v=0$ level is at a height of 906.357 cm^{-1} from the minimum of the potential energy curve) are listed in Table 4.16. For $^{14}\text{N}^{16}\text{O}$, the values of B_e , α_e and

D_e are given by Amiot and Guelachvili (1979) and that of ω_e and $\omega_e x_e$ are given by Engleman Jr. and Rouse (1971). We have calculated these values for $^{15}\text{N}^{18}\text{O}$ from the isotopic relations

$$B_e^i = \rho^2 B_e, \alpha_e^i = \rho^3 \alpha_e, D_e^i = \rho^3 D_e, \omega_e^i = \rho \omega_e, \omega_e^i x_e^i = \rho^2 \omega_e x_e^i, \quad (4.7)$$

where $\rho = (\mu/\mu^i)^{1/2}$ ($\rho=0.9552905$ for $^{15}\text{N}^{18}\text{O}$). The observed values of the molecular constants of $^{15}\text{N}^{18}\text{O}$ in the present work are compared with the calculated values in Table 4.17. The agreement between them is found to be extremely good.

While the analysis of the γ system of $^{15}\text{N}^{18}\text{O}$ was in progress, we found a reference to the work of Telfo *et al.* (1980) who have analyzed the infrared vibrational and rotational bands of $^{15}\text{N}^{18}\text{O}$. In Table 4.18, the values of B_v , D_v , A_v and A_{Dv} of the $X^1\Sigma^+$ state of $^{15}\text{N}^{18}\text{O}$ obtained in the present work are compared with the corresponding values given by Telfo *et al.* In general, the values obtained from the infrared vibration-rotation spectra recorded under higher resolution on a Fourier transform spectrometer are expected to be more accurate than those obtained from the electronic band spectra. Understandably the values given by Telfo *et al.* seem to be more accurate. A comparison of the two sets of molecular constants can be made from Table 4.18. The present B_v values agree with the corresponding values of Telfo *et al.* in the third decimal place, the D_v values (which are of the order of 10^{-6} cm^{-1}) in the first digit, the A_v values in the second decimal place, but the A_{Dv} value (which is of the order of 10^{-4} cm^{-1}) agrees in the first digit for $v=1$ and differs greatly for $v=2$. But it must be noted here that in the present work we have estimated the Λ -doubling coefficients p_v and q_v values also. These are not considered by Telfo *et al.*

Table 4.11: Rotational constants ^a (in cm^{-1}) of the 0-1, 0-2, 0-3 bands of the γ system of $^{15}\text{N}^{18}\text{O}$

Name	0-1 band	0-2 band	0-3 band
<u>A²Σ^+</u>			
B_v	1.81346(7)	1.81334(6)	1.81324(8)
$D_v \times 10^6$	4.50(5)	4.83(3)	4.41(7)
<u>X²Π_r</u>			
A_v	122.871(3)	122.713(2)	122.444(3)
$A_{D_v} \times 10^4$	0.94(5)	0.13(4)	-1.01(8)
B_v	1.53342(6)	1.51782(6)	1.50256(8)
$D_v \times 10^6$	4.44(5)	4.70(3)	4.42(7)
$p_v \times 10^3$	9.5(2)	12.2(1)	10.0(2)
$q_v \times 10^5$	-1.6(7)	7.6(4)	7.1(9)

^aNumber in the parenthesis is the uncertainty in the last digit and corresponds to one standard deviation.

Table 4.12: Band origins^a (in cm^{-1}) of the γ system of $^{15}N^{18}O$

Band	T_v' T_v''
0-1	42336.877(2)
0-2	40569.209(1)
0-3	38827.282(2)

^aNumber in the parenthesis is the uncertainty in the last digit and corresponds to one standard deviation.

Table 4.13: Merged rotational constants ^a (in *cm*⁻¹) of the X²Π and A²Σ states of ¹⁵N ¹⁸O

A ² Σ ⁺						
<i>v</i>	<i>B_v</i>	<i>D_v</i> × 10 ⁶				
0	1.81349(4)	-4.80(2)				
X ² Π						
<i>v</i>	<i>B_v</i>	<i>D_v</i> × 10 ⁶	<i>A_v</i>	<i>A_{D_v}</i> × 10 ⁴	<i>p_v</i> × 10 ²	<i>q_v</i> × 10 ⁴
1	1.53345(4)	4.73(2)	122.871(3)	1.05(5)	1.08(2)	0.32(5)
2	1.51798(4)	4.68(2)	122.714(2)	0.06(4)	1.17(1)	0.66(4)
3	1.50281(4)	4.81(2)	122.442(3)	-0.89(8)	1.03(2)	0.602(95)

^aNumber in the parenthesis is the uncertainty in the last digit and corresponds to one standard deviation.

Table 4.11: Merged band origins^a (in cm^{-1}) of the γ system of $^{15}\text{N}^{16}\text{O}$

Band	T_v' T_v''
0-1	12336.878(2)
0-2	40569.210(1)
0-3	38827.282(2)

^aNumber in the parenthesis is the uncertainty in the last digit and corresponds to one standard deviation.

Table 4.15: Equilibrium molecular constants ^a (in cm^{-1} , unless otherwise stated) of the X²Π state of ¹⁵N¹⁸O

Molecular constant	Data
ω_e	1819.15(1)
$\omega_e x_e$	12.870(2)
B_e	1.55644(4)
α_e	0.015343(5)
$D_e \cdot 10^6$	4.5574(3) ^b
$r_e(\text{\AA})$	1.15056(1)
$I_e(\text{gcm}^2) \cdot 10^{19}$	1.79854(5)

^aNumber in the parenthesis is the uncertainty in the last digit and corresponds to one standard deviation.

^bCalculated from Kratzer's relation $D_e = (4B_e^3)/(\omega_e^2)$.

Table 4.16: Vibrational term values $T_v^{a,b}$ (in cm^{-1}) of the $X^2\Pi$ and $A^2\Sigma^+$ states of $^{15}\text{N}^{18}\text{O}$

state	v	T_v
$A^2\Sigma^+$	0	44130.287(6)
$X^2\Pi$	3	5303.007(6)
	2	3561.078(9)
	1	1793.409(6)

^aNumber in the parenthesis is the uncertainty in the last digit and corresponds to one standard deviation. $T_v = T_e + G(v)$.

^bThe term values are expressed relative to the $v = 0$ level of the $X^2\Pi$ state, which is at 906.357 cm^{-1} above the minimum of its potential energy curve.

Table 4.17: Vibrational and rotational constants^a (in cm^{-1}) of the X²Π state of ¹⁴N¹⁶O and ¹⁵N¹⁸O

Constant	¹⁴ N ¹⁶ O	¹⁵ N ¹⁸ O	
		Present work	Calculated values
B_r	1.704918(8) ^b	1.5564(4)	1.555874(8)
α_r	0.01753(1) ^b	0.015343(5)	0.01528(1)
$D_r \times 10^6$	5.162(9) ^b	4.5574(3)	4.549(9)
ω_r	1904.405 ^c	1819.15(1)	1819.2598
$\omega_r r_e$	14.1870 ^c	12.870(2)	12.9468

^aNumber in the parenthesis is the uncertainty in the last digit and corresponds to one standard deviation.

^bFrom Amiot and Guelachvili(1979).

^cFrom Engleman Jr. and Rouse(1971).

Table 4.18: Comparison of the rotational constants (in cm^{-1}) of the $X^2\Pi$ state of $^{15}N^{18}O$

Values from the present work on the γ system			
v	1	2	3
B_v	1.53345(4)	1.51798(4)	1.50281(4)
$D_v \times 10^6$	-4.73(2)	-4.68(2)	-4.81(2)
A_v	122.871(3)	122.714(2)	122.442(3)
$A_{D_v} \times 10^4$	1.05(5)	0.06(4)	-0.89(8)
Values ^a from the infrared vibration-rotation bands			
v	1	2	3
B_v	1.532897(7)	1.517554(7)	1.50219(2)
$D_v \times 10^6$	4.575(5)	4.588(5)	4.63(3)
A_v	122.9107(6)	122.6688(7)	122.413(2)
$A_{D_v} \times 10^4$	1.44(3)	1.36(3)	

^aFrom Teffo *et al* (1980).

4.3 Summary

The significance of the spectra of the nitric oxide is outlined. Experimental details for the excitation of the γ ($A^2\Sigma^+ - X^2\Pi_r$) system of the isotopomers $^{14}\text{N}^{16}\text{O}$, $^{15}\text{N}^{16}\text{O}$, $^{14}\text{N}^{18}\text{O}$, and $^{15}\text{N}^{18}\text{O}$ are presented. For each of the isotopomers, six bands, each with four characteristic band heads, are observed under medium dispersion.

The γ system of $^{15}\text{N}^{18}\text{O}$ and several bands of the same system of $^{14}\text{N}^{18}\text{O}$ are observed for the first time. For each of the isotopomers the first vibrational interval $\Delta G(1/2)$ of the $A^2\Sigma^+$ state and the vibrational constants ω_e and $\omega_e x_e$ of the $X^2\Pi_r$ state were obtained from the vibrational analysis of the band heads.

The rotational structure of the 0-1, 0-2, and 0-3 bands of the γ system of $^{15}\text{N}^{18}\text{O}$ has been analyzed using the effective Hamiltonian method. The method of MERGING has been used to obtain a unique set of rotational constants for the $A^2\Sigma^+$ and $X^2\Pi_r$ states of $^{15}\text{N}^{18}\text{O}$. From the analysis, the molecular constants B_v and D_v of $A^2\Sigma^+$ and B_v , D_v , A_v , A_{Dv} , p_v and q_v of $X^2\Pi_r$ are estimated. From a plot of the Fortrat diagram for the 0-2 band it is established that the $X^2\Pi_r$ state changes from Hund's case (a) to case (b) for high J values.

Bibliography

- [1] Albritton, D.L., Schmeltekopf, A.L., and Zare, R.N. *J. Mol. Spectrosc.* **67**, 132 (1977).
- [2] Amiot, C., Bacis, R. and Guelachvili, G. *Can. J. Phys.* **56**, 251 (1978).
- [3] Amiot, C., Maillard, J.-P. and Chauville, J. *J. Mol. Spectrosc.* **87**, 196 (1981).
- [4] Amiot, C. and Guelachvili, G. *J. Mol. Spectrosc.* **76**, 86 (1979).
- [5] Audouze, J. *CNO Isotopes in Astrophysics (Dordrecht: Reidel)* 5 (1977).
- [6] "Berkeley News Letter" *Published once in two months by the Departments of Physics and Astronomy, University of California, Berkeley, U.S.A.*
- [7] Brown, J.M., Hougen, J.T., Huber, K.P., Johns, J.W.C., Kopp, I., Lefebvre-Brion, H., Merer, A.J., Ramsay, D.A., Rostas, J. and Zare, R.N. *J. Mol. Spectrosc.* **55**, 500 (1975).
- [8] Brown, J.M., Colbourn, E.A., Watson, J.K.G. and Wayne, F.D. *J. Mol. Spectrosc.* **74**, 294 (1979).
- [9] Burrows, M.D., Baughcum, S.L. and Oldenorg, R.C. *Appl. Phys. Lett.* **46**, 22 (1985).
- [10] Cisak, H., Danielak, J. and Rytel, M. *Acta Physica Polonica* **17**, 67 (1970).
- [11] Coxon, J.A. *J. Mol. Spectrosc.* **72**, 252 (1978).

- [12] Crosswhite, H.M. and Hopkins, J. *J. Spectroscopy Report No. 13, Baltimore* (1958).
- [13] Crosswhite, H.M. *J. Res. Natl. Bur. Stds., A Phys. and Chem.* **79A**, 17 (1975).
- [14] Dale, R.M., Johns, J.W.C., Mckellar, A.R.W. and Rigglin, M. *J. Mol. Spectrosc.* **67**, 440 (1977).
- [15] Edlen, B. *J. Opt. Soc. Amer.* **43** 399 (1953).
- [16] Engleman, Jr.R. and Rouse, P.E., Peck, H.M., Baiamonte, V.D. *Los Almos Scientific Laboratory, University of California report LA-4364 UC-34 Physics I* (1970).
- [17] Engleman, Jr.R. and Rouse, P.E. *J. Mol. Spectrosc.* **37**, 240 (1971).
- [18] Freedman, R. and Nicholls, R.W. *J. Mol. Spectrosc.* **83**, 229 (1980).
- [19] Gatterer, A. and Junkes, J. *In the Astrophysical Laboratory of the Vatican Observatory Second Edition* (1956).
- [20] Gilmore, F.R. *J. Quant. Spectrosc. Radiat. Transfer.* **5**, 369 (1965).
- [21] Henry, A., Le Moal, Ph.C. and Valentin, A. *J. Mol. Spectrosc.* **70**, 18 (1978).
- [22] Herzberg, G. *Molecular Spectra and Molecular Structure, Vol.I (Spectra of Diatomic Molecules), 2nd ed., D. Van Nostrand Company, Inc., New York* (1950).
- [23] Herzberg, G. *Molecular Spectra and Molecular Structure, Vol.I (Spectra of Diatomic Molecules), third ed., D. Van Nostrand Company, Inc., New York* (1971).
- [24] Huber, K.P. and Herzberg, G. *Molecular Spectra and Molecular Structure Constants of Diatomic Molecules* (1979).

- [25] Kivel, B., Mayer, H. and Bethe, H. *Ann. Phys.* **2**, 57 (1957).
- [26] Kopp, I. and Hougen, J.T. *Can. J. Phys.* **45**, 2581 (1967).
- [27] Langhoff, S.P., Bauschlicher, Jr. C.W. and Partridge, H. *J. Chem. Phys.* **89**, 4909 (1988).
- [28] McDermid, I.S. and Laudenslager, J.B. *J. Quant. Spectrosc. Radiat. Transfer.* **27**, 483 (1982).
- [29] Meerts, W.L. and Dymannus, A. *J. Mol. Spectrosc.* **44**, 320 (1972).
- [30] Miescher, E. and Huber, K.P. *Spectroscopy, M.T.P. International Reviews of Science, Physical Chemistry Series 2, Vol. 3. Edited by D.A. Butterworths, London, England* (1976)
- [31] Mulliken, R.S. *Rev. Mod. Phys.* **3**, 89 (1931).
- [32] Mulliken, R.S. *Rev. Mod. Phys.* **4**, 1 (1932).
- [33] Patel, C.K.N. and Kerl, R.J. *Optics Communication* **24**, 294 (1978)
- [34] Prasad, C.V.V. *Ph.D. Thesis, Memorial University of Newfoundland* (1987).
- [35] Prasad, C.V.V. and Reddy, S.P. *J. Mol. Spectrosc.* **130**, 62 (1988).
- [36] Reddy, S.P. and Prasad, C.V.V. *J. Phys. E: Sci. Instrum.* **22**, 306 (1989).
- [37] Shenstone, A.G. *J. of the Optical Society of America* **45** 868 (1955).
- [38] Strutt, R.J. *R.P.S.* **93** 254 (1917).
- [39] Telfo, J.L., Henry, A., Cardinet, Ph. and Valentin, A. *J. Mol. Spectrosc.* **82**, 348 (1980).

- [40] Valentin, A., Henry, Ph.C., Le Moal, M.F., Chen, Dawu and Rao, K.H. *J. Mol. Spectrosc.* **70**, 9 (1978).
- [41] Zare, R.N., Schmeltekopf, A.L., Harrop, W.J. and Albritton, D.L. *J. Mol. Spectrosc.* **46**, 37 (1973).

